Dimers and circle patterns

Richard Kenyon, Wai Yeung Lam, Sanjay Ramassamy, Marianna Russkikh

DIMERS AND CIRCLE PATTERNS

RICHARD KENYON, WAI YEUNG LAM, SANJAY RAMASSAMY, MARIANNA RUSSKIKH

Abstract. We establish a correspondence between the dimer model on a bipartite graph and a circle pattern with the combinatorics of that graph, which holds for graphs that are either planar or embedded on the torus. The set of positive face weights on the graph gives a set of *global coordinates* on the space of circle patterns with embedded dual. Under this correspondence, which extends the previously known isoradial case, the urban renewal (local move for dimer models) is equivalent to the Miquel move (local move for circle patterns). As a consequence the Miquel dynamics on circle patterns is governed by the octahedron recurrence. As special cases of these circle pattern embeddings, we recover harmonic embeddings for resistor networks and s-embeddings for the Ising model.

Contents

1. Introduction

The *bipartite planar dimer model* is the study of random perfect matchings ("dimer coverings") of a bipartite planar graph. Natural parameters for the dimer model, defining the underlying probability measure, are *face weights*, which are positive real parameters on the bounded faces of the graph [13]. The dimer model is a classical statistical mechanical model, and can be "solved" using determinantal methods: partition functions and correlation kernels are computed by determinants of associated matrices defined from the weighted graph [17]. Several other two-dimensional statistical models, including the Ising model and the spanning tree model, can be regarded as special cases of the dimer model by subdividing the underlying graph [8, 22]. A question raised in [13] concerns how to relate the parameters (the face weights of the dimer model) to some geometric property of the underlying graph or embedding. In [28, 18], a certain family of graph embeddings and associated weights, called *isoradial graphs*, was shown to lead to important simplifications in the probability model (an *isoradial* embedding is one where every face is cyclic with circumcircle of radius 1). We generalize this construction here, associating to a face-weighted bipartite planar graph a *circle pattern*: a realization of the graph in $\mathbb{C}$ with cyclic faces where all vertices on a face lie on a circle[1]. This realization has the following important features:

(1) It generalizes the isoradial case.
(2) Local rearrangements of the graph, called *urban renewals* or *spider moves* or *cluster mutations*, correspond to applications of the Miquel six-circles theorem for the underlying circle pattern.
(3) Planar resistor networks can be subdivided into bipartite planar graphs with face weights. Our construction of circle patterns is compatible with harmonic embeddings of the network.
(4) The (ferromagnetic) Ising model on a planar graph can be associated with dimers on a related bipartite planar graph. Our construction is compatible with the s-embedding of the associated Ising model [6, 27].

The circle patterns arising under this correspondence are those with bipartite graph and with an *embedded dual*, where the dual graph is the graph of circle centers. The set of circle patterns with embedded dual includes all embedded circle patterns in which each face contains the center, but may miss other embedded circle patterns; moreover having embedded dual does not imply that the primal pattern is embedded.

Circle patterns are related, through stereographic projection, to 3-dimensional ideal hyperbolic polyhedra. The problem of existence and uniqueness of such polyhedra with fixed combinatorics and dihedral angles is a well-studied nonlinear problem [35, 5]. On the space of circle patterns with fixed bipartite graph $\mathcal{G}$ and embedded dual we define a set of global coordinates (the face variables of the underlying graph), for which the

[1]Our circle patterns are not necessarily embedded. An *embedded circle pattern* is a more restrictive object, when the realization is an actual embedding of the graph.

existence and uniqueness problem becomes essentially *linear*. Note that the space of patterns with embedded dual coincides with the space of crease patterns of origami that are locally flat-foldable [15].

Our construction extends to infinite, bi-periodic bipartite planar networks, in which case we get periodic (and quasiperiodic) circle patterns. When $\mathcal{G}$ is the infinite square grid we consider *Miquel dynamics*, a discrete-time dynamical system for periodic circle patterns introduced in [34] and also studied in [12], which we show is equivalent to the octahedron recurrence, hence belongs to the class of discrete integrable systems.

We note that the correspondence between the dimer model and circle pattern embeddings should include a third type of object, namely a three-dimensional inscribed polyhedron, in a spirit similar to the Maxwell-Cremona correspondence [39] between polyhedra and harmonic embeddings. We will not, however, pursue this connection in this paper.

In the dimer model our natural parameters, which are face weights, are positive. Moreover whenever a circle pattern is embedded, it leads to positive face weights. However in some circumstances it is useful to allow general real weights as well; in particular the Miquel dynamics is algebraic in nature and the sign of the weights does not typically matter.

Circle center realizations are also considered in [7] under the name of t-embeddings with an emphasis on the convergence of discrete holomorphic functions to continuous ones in the small mesh size limit, i.e., when the circle radii tend to 0.

During the completion of this work, a preprint by Affolter [2] appeared, which shows how to go from circle patterns to dimers and observes that the Miquel move was governed by the central relation. Affolter notes that there is some information missing to recover the circle pattern from the X variables. We provide here a complete picture.

Organization of the paper. In Section 3, we introduce circle pattern embeddings associated with bipartite graphs with positive face weights in the planar case. Section 4 is devoted to circle pattern embeddings in the torus case. In Section 5 we show the equivalence between the spider move for the bipartite dimer model and the central move coming from Miquel's theorem for circle patterns. In particular this gives a cluster algebra structure underlying Miquel dynamics. Section 6 is devoted to translating into planar geometry the generalized Temperley bijection between resistor networks and dimer models. Finally in Section 7 we show that Chelkak's s-embeddings for the Ising model [6] arise as a special case of our circle pattern embeddings.

2. Background on dimers and the Kasteleyn matrix

For general background on the dimer model, see [19]. A *dimer cover*, or *perfect matching*, of a graph is a set of edges with the property that every vertex is contained in exactly one edge of the set. If $\nu : E \to \mathbb{R}_{>0}$ is a positive weight function on edges, we associate a weight $\nu(m) = \prod_{e\in m} \nu(e)$ to a dimer cover which is the product of its edge weights. We can also associate to this data a probability measure μ on the set M of dimer covers, giving a dimer cover m a probability $\frac{1}{Z}\nu(m)$, where $Z = \sum_{m\in M} \nu(m)$ is a normalizing constant, called the *partition function*.

Two weight functions ν_1, ν_2 are said to be *gauge equivalent* if there is a function $F : V \to \mathbb{R}$ such that for any edge vw, $\nu_1(vw) = F(v)F(w)\nu_2(vw)$. Gauge equivalent weights define the same probability measure μ. For a planar bipartite graph, two weight functions are gauge equivalent if and only if their *face weights* are equal, where the face weight of a face with vertices $w_1, b_1, \dots, w_k, b_k$ is

$$X = \frac{\nu(w_1b_1)\dots\nu(w_kb_k)}{\nu(b_1w_2)\dots\nu(b_kw_1)}. \tag{1}$$

If $\mathcal{G}$ is a planar bipartite graph which has dimer covers, a *Kasteleyn matrix* is a signed, weighted adjacency matrix, with rows indexing the white vertices and columns indexing the black vertices, with $K(w, b) = 0$ if w and b are not adjacent, and $K(w, b) = \pm\nu(w, b)$ otherwise, where the signs are chosen so that the product of signs is $(-1)^{k+1}$ for a face of degree $2k$. Kasteleyn [16] showed that the determinant of a Kasteleyn matrix is the weighted sum of dimer covers:

$$Z = |\det K| = \sum_{m\in M} \nu(m).$$

Different choices of signs satisfying the Kasteleyn condition correspond to multiplying K on the right and/or left by diagonal matrices with ±1 on the diagonals. Different choices of gauge correspond to multiplying K on the right and left by diagonal matrices with positive diagonal entries (see e.g. [13]). Note that in terms of any (gauge equivalent) Kasteleyn matrix we can recover the face weights via the formula

$$X = (-1)^{k+1}\frac{K(w_1, b_1)\dots K(w_k, b_k)}{K(w_2, b_1)K(w_3, b_2)\dots K(w_1, b_k)}. \tag{2}$$

In some circumstances it is convenient to take complex signs $e^{i\theta}$ in the Kasteleyn matrix, rather than just ±1; in that case the required condition on the signs is that the quantity X in (2) is positive, see [32]. This generalization will be used below.

Certain elementary transformations of $\mathcal{G}$ preserve the measure μ; see Figure 1.

3. Bipartite graphs and circle patterns

In this section, we establish a correspondence between bipartite graphs with positive face weights and circle patterns with embedded dual. While the construction can be extended to general real weights, certain aspects are nicer in the positive weight case, in particular the embedding property of the dual graph (Theorem 2 below).

3.1. **Centers of circle patterns.**

Centers of circle patterns with bipartite vertices in the plane have been considered in various forms. In [33, 31], they are called conical meshes and related to discrete minimal surfaces [26]. In terms of origami, they are the crease patterns that are locally flat-foldable [15].

Here we recall the main property of the centers. Suppose $z : V \to \mathbb{C}$ is an embedding of a bipartite graph $\mathcal{G}$ with cyclic faces, except perhaps the outer face, which we assume convex. Assume also that each bounded face contains its circumcenter. The circumcenters form an embedding of the dual graph $u : F \to \mathbb{C}$, except for the outer dual vertex f_o. Since each dual edge connects the centers of two circles with the

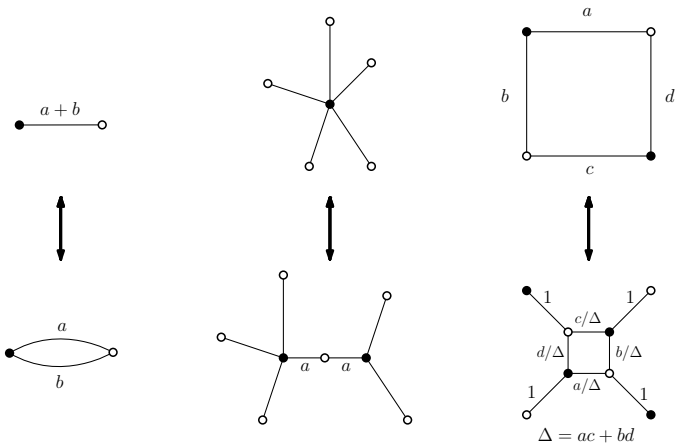

FIGURE 1. Elementary transformations preserving the dimer measure μ. 1. Replacing parallel edges with weights a, b by a single edge with weight $a + b$; 2. contracting a degree 2 vertex whose edge have equal weights; the spider move, with weights transformed as indicated.

corresponding primal edge as a common chord, each dual edge is a perpendicular bisector of the primal edge. We define the outer dual vertex to be $u_{f_o} = \infty$; then for each dual edge $f f_o$ we define its embedding to be the ray from u_f to ∞, perpendicular to the corresponding primal edge, and directed outward away from the rest of the graph. Under the assumption that the graph is bipartite, note that the alternating sum of angles around every dual vertex is zero. Moreover note that the faces of the dual graph, including the unbounded faces, are convex: thus we have a *convex embedding*, that is, an embedding with convex faces.

The converse to this construction also holds:

Proposition 1. *Suppose $\mathcal{G} = (V, E, F)$ is a bipartite graph and $u : F \to \mathbb{C}$ is a convex embedding of the dual graph (with the outer vertex at ∞). Then there exists a circle pattern $z : V \to \mathbb{C}$ with u as centers if and only if the sum of alternate angles around every dual vertex is π.*

Note also that we don't require z to be an embedding, only a realization with the property that vertices on each face lie on a circle. It seems difficult to give conditions under which z will be an embedding, although the space of circle pattern embeddings is an open subset of our space of realizations.

Proof. It remains to show that given such an embedding u, there is a circle pattern with u as centers. We construct such a circle pattern z as follows. Pick a vertex i and assign the vertex to some arbitrary point z_i in the plane. We then define z_j for a neighboring vertex j in such a way that z_j is the image of z_i under reflection across the line connecting the neighboring dual vertices. Because of the angle condition, iteratively defining the z value around a face will return to the initial value. Hence the map z is well defined and independent of the path chosen. □

3.2. **From circle patterns to face weights.** Suppose we have an embedded circle pattern $z : \mathcal{G} \to \mathbb{C}$, in which each bounded face contains its circumcenter, with outer face also cyclic, and with the combinatorics of a planar bipartite graph $\mathcal{G}$. Let $u : F \to \mathbb{C}$ be the circle centers, with the outer dual vertex u_{f_o} at its circumcenter.

Now define a function $\omega(wb) = u_l - u_r$ where l, r denote the left and the right face of the edge wb oriented from w to b (if one of u_l, u_r is the outer vertex we use the *negative* of this, $u_r - u_l$). We think of ω as a 1-form, or flow, that is, a function on oriented edges changing sign under change of orientation. Define a matrix K with rows indexing the white vertices and columns indexing the black vertices by $K(w, b) = \omega(wb)$. We claim that K is a Kasteleyn matrix (with complex signs). To see this, suppose a face f with center u has vertices $w_1 b_1 \dots w_k b_k$ in counterclockwise order. We denote the centers of the neighboring faces as $u_1, u_2, \dots, u_{2k}$. Then

$$\frac{K_{w_1 b_1} K_{w_2 b_2} \dots K_{w_k b_k}}{K_{w_1 b_0} K_{w_2 b_1} \dots K_{w_k b_{k-1}}} = \frac{(u_2 - u)(u_4 - u) \dots (u_{2k} - u)}{(u - u_1)(u - u_3) \dots (u - u_{2k-1})}$$

where $b_0 = b_k$. Hence, by the angle condition, the face weight

$$X_f := (-1)^{k+1} \frac{(u_2 - u)(u_4 - u) \dots (u_{2k} - u)}{(u - u_1)(u - u_3) \dots (u - u_{2k-1})} = (-1)^{k+1} \frac{K_{w_1 b_1} K_{w_2 b_2} \dots K_{w_k b_k}}{K_{w_1 b_0} K_{w_2 b_1} \dots K_{w_k b_{k-1}}} \tag{3}$$

is positive and K is a Kasteleyn matrix. This associates a positive face-weighted bipartite planar graph to a circle pattern.

3.3. **Canonical gauge for finite planar graphs with outer face of degree 4.** In this section we start with a face weighted bipartite planar graph (with outer face of degree 4 and which has dimer covers) and a convex quadrilateral P, and construct a circle pattern with dual embedded in P. See Figure 2 for an example. Our inductive construction will in principle work for graphs with outer face of higher degree, but the initial step of the induction proof is more complicated and is not something we currently can handle.

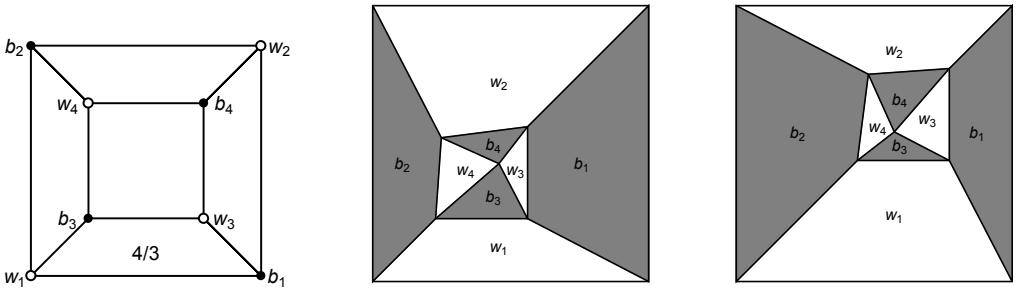

FIGURE 2. The "cube" graph on the left (with all face weights 1 except the one indicated with weight 4/3) is embedded as a circle pattern with the dual graph of circle centers having outer boundary a square; both solutions are shown on the right.

Let $\mathcal{G}$ be an embedded bipartite planar graph, with outer face of degree 4 with vertices w_1, b_1, w_2, b_2, and which has dimer covers. We also assume $\mathcal{G}$ is *nondegenerate*,

that is, each edge occurs in at least one dimer cover, and $\mathcal{G}$ is *well-connected*: removing one white and one black boundary vertex, or removing all boundary vertices, the remaining graph still has dimer covers. Let $X : F \to \mathbb{R}_{>0}$ be a positive real number associated to each bounded face. Let $P \subset \mathbb{R}^2$ be a convex quadrilateral, with edges $W_1, B_1, W_2, B_2 \in \mathbb{C}$ summing to zero.

We add one more vertex v_∞ to $\mathcal{G}$ "at infinity" and an edge from the four outer vertices to this vertex. Let $\mathcal{G}^*$ be the dual graph of this augmented graph $\mathcal{G} \cup \{v_\infty\}$. This $\mathcal{G}^*$ has outer face of degree 4. Denote the vertices of the outer face by f_{11}, f_{12}, f_{21} and f_{22}, where f_{ij} is adjacent to the edge $(w_i b_j)^*$.

We construct a convex embedding in P of $\mathcal{G}^*$, with the outer vertices of $\mathcal{G}^*$ going to the vertices of P, satisfying the property that the vertices of $\mathcal{G}^*$ go to the circle centers of a circle pattern with the combinatorics of $\mathcal{G}$ (in the sense that the angles satisfy Proposition 1), and moreover the face variables X_f of $\mathcal{G}$ give the "alternating product of edge lengths" as in (1).

Let K be a Kasteleyn matrix associated to $\mathcal{G}$ (without the vertex v_∞) with face weights X. Let $G(w)$ and $F(b)$ be functions on white and black vertices of $\mathcal{G}$ such that for all internal white vertices w, we have

$$\sum_b G(w) K_{wb} F(b) = 0, \tag{4}$$

and for all internal black vertices b, we have

$$\sum_w G(w) K_{wb} F(b) = 0, \tag{5}$$

and for $i = 1, 2$

$$\sum_w G(w) K_{wb_i} F(b_i) = B_i \tag{6}$$

$$\sum_b G(w_i) K_{w_i b} F(b) = -W_i. \tag{7}$$

Functions G, F satisfying (4) and (5) are said to give a *canonical gauge* for $\mathcal{G}$. The existence of canonical G, F, for general boundary lengths, satisfying the boundary conditions (6),(7) is discussed in Section 3.4 below. As shown there the equations (4)-(7) determine G and F up to a finite number of choices: in fact typically two choices for boundary length 4.

Given G, F satisfying the above, define a function ω on edges by $\omega(wb) = G(w) K_{wb} F(b)$ (and $\omega(bw) = -\omega(wb)$, so that ω is a 1-form).

The equations (4) and (5) imply that ω is co-closed (divergence free) at internal vertices. Thus ω can be integrated to define a mapping ϕ from the dual graph $\mathcal{G}^*$ into $\mathbb{C}$ by the formula

$$\phi(f_1) - \phi(f_2) = \omega(wb) \tag{8}$$

where f_1, f_2 are the faces adjacent to edge wb, with f_1 to the left and f_2 to the right when traversing the edge from w to b. The mapping ϕ is defined up to an additive

constant; we choose the constant so that the vertices $f_{11}, f_{12}, f_{22}, f_{21}$ go to the vertices of P.

Theorem 2. *Suppose $\mathcal{G}$ has outer face of degree 4. The mapping ϕ defines a convex embedding into P of $\mathcal{G}^*$ sending the outer vertices to the corresponding vertices of P. Moreover, the images of the vertices of $\mathcal{G}^*$ are the centers of a circle pattern with the combinatorics of $\mathcal{G}$, including the outer face, that is, the outer face of $\mathcal{G}$ will also be cyclic.*

Boundary length 4 is special in the sense that if $\mathcal{G}$ has outer face of degree strictly larger than 4, the outer face of the associated circle pattern will not necessarily be cyclic.

Proof. We rely on a Theorem of D. Thurston [37]: any nondegenerate, well-connected planar bipartite graph with four marked boundary vertices w_1, b_1, w_2, b_2 can be built up from the 4-cycle graph with vertices w_1, b_1, w_2, b_2 using a sequence of *elementary transformations* (see Figure 1); moreover the marked vertices remain in all intermediate graphs.

Therefore to complete the proof it remains to show that, first, the result holds when $\mathcal{G}$ is the simplest graph: a single 4-cycle with only the vertices w_1, b_1, w_2, b_2 in that order, and second, if it holds for a graph then it holds for any elementary transformation applied to that graph.

To use this argument we must extend slightly our notion of convex embedding to include the case when $\mathcal{G}$ has degree 2 vertices, and when $\mathcal{G}$ has parallel edges, because these necessarily occur at intermediate stages when we build up the graph $\mathcal{G}$ from the 4-cycle.

When $\mathcal{G}$ has parallel edges connecting two vertices w and b, the dual graph $\mathcal{G}^*$ has one or more degree-2 vertices there; we do not assign a location to these vertices since the circles they correspond to are not defined; rather, we simply embed $\mathcal{G}^*$ as if those parallel edges were joined into a single edge.

When $\mathcal{G}$ has a degree-2 vertex v, connected to neighbors v_1 and v_2, then for the associated canonical 1-form ω we necessarily have $\omega_{vv_1} + \omega_{vv_2} = 0$. This implies that under ϕ the duals of these edges get mapped to the same edge. We call this a "near-embedding" since faces of degree 2 in $\mathcal{G}^*$ get collapsed to line segments. Note however that for any such graph $\mathcal{G}$, contracting degree-2 vertices results in a new graph with the same mapping ϕ, minus those paired edges.

Consequently, among the elementary transformations of Figure 1, only the spider move has a nontrivial effect on the embedding.

Now let $\mathcal{H}$ be a graph obtained from $\mathcal{G}$ by applying a spider move. The embedding of $\mathcal{H}$ is obtained from the embedding of $\mathcal{G}$ by a "central move", see (14) below. This move gives a convex embedding by convexity of the faces: the new central vertex is necessarily in the convex hull of its neighbors: see Lemma 3 below.

For the case $\mathcal{G}$ is a 4-cycle, see Lemma 3 and Figure 3.

Finally, the fact that ϕ maps the vertices of $\mathcal{G}^*$ to centers of a circle pattern follows from the proof of Proposition 1 and the fact that the sum of the angles of the corners of the white/black faces around a given vertex of $\phi(\mathcal{G}^*)$ equals π. The fact that the

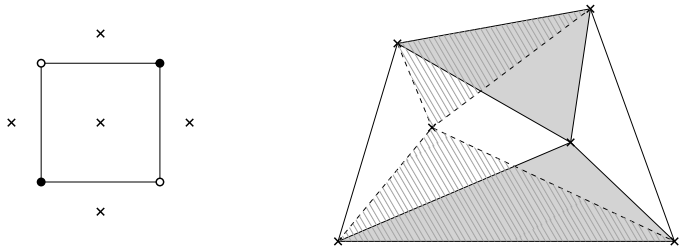

FIGURE 3. For the 4-cycle equation (9) defines two solutions, shown for a particular choice of boundary.

outer face is cyclic also follows by induction: this is true for the 4-cycle, and the central moves do not move the outer dual vertices, or change their radii. □

We now treat the base case of the induction in the above proof, namely the case of the 4-cycle.

Lemma 3. *Let Q be a convex quadrilateral with vertices $0, 1, z, w$ in counterclockwise order and let $X \in (0, \infty)$. The equation*

$$-\frac{(1-u)(w-u)}{(0-u)(z-u)} = X \tag{9}$$

has two solutions u (counted with multiplicity), both of which lie strictly inside Q.

Proof. When $X = 0$ the solutions to (9) are $u = 1, u = w$ and when $X = \infty$ the two solutions are $u = 0, u = z$. Notice that no other point on the boundary of Q can be a solution for any X because the one of the angle sums $0u1 + zuw$ or $1uz + wu0$ would be larger than π. So by continuity it suffices to show that for small $X > 0$ there is one solution inside Q near 1 and one solution inside Q near w. Solving (9) for u and expanding near $X = 0$ gives the solutions

$$u = 1 - \frac{z-1}{w-1}X + O(X^2)$$
$$u = w - w\frac{z-w}{1-w}X + O(X^2).$$

Note that for the first solution, $\arg\frac{w-1}{z-1}$ is less than the angle at 1 of Q, so the vector $-\frac{z-1}{w-1}$ points into Q from the point 1; thus this solution is inside Q for small $X > 0$. For the second, $\arg\frac{z-w}{1-w}$ is less than the angle of Q at w, so the vector $-w\frac{z-w}{1-w}$ points into the interior of Q from w. □

Remark 4. *The* isogonal conjugate *of a point U with respect to a quadrilateral $ABCD$ is constructed by reflecting the lines UA, UB, UC and UD about the angle bisectors of A, B, C, and D respectively. If these four reflected lines intersect at one point, then this point is called the isogonal conjugate of U. Not all points have an isogonal conjugate with respect to a quadrilateral, but only those lying on a certain cubic curve associated with the quadrilateral* [4]*. One can show that the two solutions to (9) are isogonally conjugate with respect to Q. Moreover all possible pairs of isogonal conjugate points inside Q can be achieved upon varying $X > 0$.*

3.4. **Existence of canonical gauge.** In this subsection we consider the case when the outer face of the planar bipartite graph has an arbitrary degree. We prove the existence of at least one canonical gauge in this setting.

Lemma 5. *For boundary of degree $2k \geq 2$, a solution to (4)-(7) exists for generic boundary values $(\vec{B}, \vec{W})$ satisfying $\sum_{i=1}^{k} B_i + \sum_{i=1}^{k} W_i = 0$.*

Proof. Let K be an invertible matrix. For an n-tuple $\vec{x} = (x_1, \dots, x_n)$ let $D_{\vec{x}}$ be the corresponding $n \times n$ diagonal matrix with entries $D_{ii} = x_i$. Let $\Psi : \mathbb{C}^{2n} \to \mathbb{C}^{2n}$ be the map from a pair of n-tuples $\vec{x}, \vec{y} = (x_1, \dots, x_n), (y_1, \dots, y_n)$ to the set of row and column sums of $D_{\vec{x}} K D_{\vec{y}}$, that is

$$\Psi(\vec{x}, \vec{y}) = (\vec{p}, \vec{q})$$

where $p_i = \sum_j x_i K_{i,j} y_j$ and $q_j = \sum_i x_i K_{i,j} y_j$. It is clear that the image of Ψ is contained in the hyperplane

$$\Sigma = \left\{ (p_1, \dots, p_n, q_1, \dots, q_n) \in \mathbb{C}^{2n} \;\middle|\; \sum_{i=1}^{n} p_i = \sum_{i=1}^{n} q_i \right\}.$$

Since Ψ is algebraic, it suffices to show that the Jacobian of Ψ is of maximal rank $2n-1$ at some point: this implies that the interior of $\Psi(\mathbb{C}^{2n})$ is not empty, hence due to the Chevalley theorem [14, 1.8.4] there exists a proper algebraic subvariety $\tilde{\Sigma}$ of Σ such that for any $(\vec{p}, \vec{q}) \in \Sigma \setminus \tilde{\Sigma}$ there exist $(\vec{x}, \vec{y})$ such that $\Psi(\vec{x}, \vec{y}) = (\vec{p}, \vec{q})$.

We can write Ψ as a composition $\Psi = \Psi_2 \circ \Psi_1$ where

$$\Psi_1(\vec{x}, \vec{y}) = (\vec{x}, \vec{p})$$

and

$$\Psi_2(\vec{x}, \vec{p}) = (\vec{p}, \vec{Q})$$

with

$$Q_j = \sum_l x_l K_{lj} \sum_i (K^{-1})_{ji} \frac{p_i}{x_i}.$$

Note that the map Ψ_1 is invertible since given $\vec{p}$ and $\vec{x}$ one can reconstruct $\vec{y}$. So it remains to find a point where the Jacobian of Ψ_2 has maximal rank. Let $p_1 = 1$ and $p_2 = \cdots = p_n = 0$. For this particular choice of $\vec{p}$ we get

$$\Psi_2(\vec{x}, \vec{p}) = (\vec{p}, \vec{Q}), \quad \text{with} \quad Q_j = (K^{-1})_{j,1} \frac{p_1}{x_1} \sum_l x_l K_{lj}.$$

Note that the right-hand side of the equation is linear in $x_2, \dots, x_n$. Since the matrix K is invertible we conclude that the Jacobian of the map that send $\vec{x}$ to $\vec{Q}$ is of rank $n-1$. Hence the Jacobian of Ψ_2 is of rank $2n-1$. To finish the proof consider $\vec{p} = (B_1, B_2, \dots, B_k, 0, \dots 0)$, $\vec{q} = (-W_1, -W_2, \dots, -W_k, 0, \dots 0)$, and let K be a Kasteleyn matrix of $\mathcal{G}$. □

Question: How many solutions are there? This number is a function only of the graph $\mathcal{G}$, and is invariant under elementary transformations preserving the boundary.

4. Biperiodic bipartite graphs and circle patterns

In this section we deal with the case of a bipartite graph embedded on a torus, or equivalently a biperiodic planar graph.

4.1. **Embedding of $\mathcal{G}^*$.** Let $\mathcal{G}$ be a bipartite graph embedded on a torus T, with complementary regions (faces) which are disks, having dimer covers, and nondegenerate. Let $\nu : E \to \mathbb{R}_{>0}$ be a set of positive edge weights. We fix two cycles l_1 and l_2 in the dual graph $\mathcal{G}^*$ which together generate the homology $H_1(T, \mathbb{Z})$, and have intersection number $l_1 \wedge l_2 = +1$.

We define new edge weights on $\mathcal{G}$ by multiplying, for $i = 1, 2$, each original edge weight by λ_i (resp. λ_i^{-1}) if the edge crosses l_i with white vertex to its left (respectively right). Define $K(\lambda_1, \lambda_2)$ to be a Kasteleyn matrix of $\mathcal{G}$ with the new edge weights and define a Laurent polynomial P by $P(\lambda_1, \lambda_2) := \det K(\lambda_1, \lambda_2)$.

The *spectral curve of the dimer model on* $\mathcal{G}$ is defined to be the zero-locus of P in $(\mathbb{C}^*)^2$. The *amoeba* of P is the image in $\mathbb{R}^2$ of the spectral curve under the mapping $(\lambda_1, \lambda_2) \mapsto (\log|\lambda_1|, \log|\lambda_2|)$. The spectral curve is a *simple Harnack curve* [21]; this has the following consequences (see [29]). Every point (λ_1, λ_2) of the spectral curve is a simple zero of $P(\lambda_1, \lambda_2)$ or it is a double zero which is then real (a real node). The derivatives P_{λ_1} and P_{λ_2} vanish only at real points, and vanish simultaneously only at real nodes; The quantity $\zeta := \frac{\lambda_2 P_{\lambda_2}}{\lambda_1 P_{\lambda_1}}$ is the *logarithmic slope* and is real exactly on the boundary of the amoeba. At a real node the logarithmic slope ζ has exactly two limits, which are nonreal and conjugate.

When (λ_1, λ_2) is a simple zero, $(\bar{\lambda}_1, \bar{\lambda}_2)$ is also a zero of $P(\lambda_1, \lambda_2)$, and in this case it is shown in [20] that $K(\lambda_1, \lambda_2)$ has a kernel which is one-dimensional. Hence there exists a pair of functions (F, G) unique up to scaling, with F defined on black vertices and G defined on white vertices, with $F \in \ker K(\lambda_1, \lambda_2)$ and $G \in \ker K^t(\lambda_1, \lambda_2)$. When λ_1, λ_2 are not both real we call it an *interior* simple zero, it corresponds to a point in the interior of the amoeba, but not at a node.

At a real node, λ_1 and λ_2 are both real and the kernel of $K(\lambda_1, \lambda_2)$ is two-dimensional. The kernel is spanned by the limits of the kernels for nearby simple zeros and their conjugates. Let F, G be functions in the kernel of $K(\lambda_1, \lambda_2)$ (resp. of $K^t(\lambda_1, \lambda_2)$) which are limits of those for simple zeros for which $\operatorname{Im}\zeta > 0$.

Let $\tilde{\mathcal{G}}$ be the lift of $\mathcal{G}$ to the plane (the universal cover of the torus). Let p_1, p_2 be the horizontal and vertical periods of $\tilde{\mathcal{G}}$ corresponding to l_1, l_2 respectively. We extend F and G to $\tilde{\mathcal{G}}$ by

$$F(b + p_{1,2}) = \lambda_{1,2} F(b), \quad G(w + p_{1,2}) = \lambda_{1,2}^{-1} G(w). \tag{10}$$

We define two co-closed 1-forms

$$\omega(wb) = G(w) K_{wb}(\lambda_1, \lambda_2) F(b) \quad \text{and} \quad \hat{\omega}(wb) = \overline{G(w)} K_{wb}(\lambda_1, \lambda_2) F(b) \tag{11}$$

and use them to define two mappings $\phi, \hat{\phi} : \tilde{\mathcal{G}}^* \to \mathbb{C}$ using (8).

Remark 6. *The mapping ϕ is periodic, in the sense that $\phi(v + p_{1,2}) = \phi(v) + V_{1,2}$ for constant vectors V_1, V_2. Indeed,*

$$F(b + p_1) G(w + p_1) = F(b) G(w) \tag{12}$$

and similarly for p_2. In the case of a real node, λ_1 and λ_2 are real hence (12) *holds with G replaced with $\bar{G}$ so $\hat{\phi}$ is also periodic.*

As a consequence of Remark 6, one can project the centers down to a flat torus and one can give an explicit formula for the aspect ratio of that torus:

Proposition 7. *The periods V_1 and V_2 of ϕ are nonzero as long as P_{λ_1} and P_{λ_2} are nonzero, and can also be chosen nonzero at a real node by an appropriate scaling. The ratio of the periods is $V_2/V_1 = \zeta = \frac{\lambda_2 P_{\lambda_2}}{\lambda_1 P_{\lambda_1}}$.*

Proof. For a matrix M we have the identity $\frac{\partial(\det M)}{\partial M_{i,j}} = M^*_{i,j}$, where $M_{i,j}$ is the (i,j)-entry of M and $M^*_{i,j}$ is the corresponding cofactor. Recalling that $P = \det K$, we have

$$\lambda_1 \frac{\partial P}{\partial \lambda_1} = \sum_{\gamma_1} \pm K(w,b) K^*(b,w)$$

where the sum is over edges crossing γ_1 (i.e. those edges of $\mathcal{G}$ with a weight involving $\lambda_1^{\pm 1}$), the sign is given by the corresponding exponent of λ_1 for that edge, and K^* is the cofactor matrix. When (λ_1, λ_2) is a simple zero of P, we have $K^*K = KK^* = (\det K)\,\mathrm{Id} = 0$ and hence the columns of K^* are multiples of F and the rows are multiples of G. In particular, we can write $K^*(b,w) = cF(b)G(w)$ for some scale factor c. We find

$$\lambda_1 \frac{\partial P}{\partial \lambda_1} = c \sum_{\gamma_1} \pm K(w,b) F(b) G(w) = cV_1.$$

Similarly

$$\lambda_2 \frac{\partial P}{\partial \lambda_2} = cV_2$$

and we conclude by taking the ratio of these.

If (λ_1, λ_2) is a node, we can take a limit of nearby simple zeros with, say, $\mathrm{Im}(\zeta) > 0$, and scaling so that V_1 is of constant length; since ζ has a well-defined nonreal limit, V_2 will also have a limit of finite length. □

Theorem 8. *The realization ϕ is a periodic convex embedding of $\tilde{\mathcal{G}}^*$, dual to a circle pattern.*

Proof. If (λ_1, λ_2) is an interior simple zero, then we show in Lemma 12 below that the realization ϕ_1 defined from $\mathrm{Re}(G(w))K_{wb}F(b)$ is a "T-graph embedding" (see definition there), mapping each white face to a convex polygon. (This result is stated in [23] without proof). In particular for ϕ_1 the sum of the angles of white polygons at vertices of $\tilde{\mathcal{G}}^*$ is π. This implies that for the realization defined by ϕ, the sum of angles of the white polygons at vertices of $\tilde{\mathcal{G}}^*$ is also π, since these polygons are simply scaled copies of those for ϕ_1. Likewise the realization ϕ_2 defined from $G(w)K_{wb}\,\mathrm{Re}(F(b))$ is a T-graph embedding, mapping each black face to a convex polygon. It suffices to show that the orientations of ϕ_1 and ϕ_2 agree. Note that the realization defined by $\overline{G(w)}K_{wb}\,\mathrm{Re}(F(b))$ is also a T-graph embedding with the *reverse* orientation to that of ϕ_2. Thus the orientations of the white and black faces agree in exactly one of ϕ or $\hat{\phi}$.

We claim that they agree in ϕ, not $\hat{\phi}$. This is a consequence of Lemma 9 below. Thus ϕ is a local homeomorphism.

By Remark 6 and Proposition 7, ϕ is periodic with nonzero periods (at interior simple zeros the P_{λ_i} are nonzero) and so ϕ is proper, and thus a global embedding (a proper local homeomorphism is a covering map).

If (λ_1, λ_2) is a double zero then one can argue similarly as above; the question of orientation is resolved by taking a limit of simple zeros, since the embeddings depend continuously on (λ_1, λ_2). □

4.2. **The circles.** Let ϕ be the embedding of $\mathcal{G}^*$ defined from ω in (11), and $\hat{\phi}$ the realization defined from $\hat{\omega}$. The boundedness of the radii in the circle pattern can be read from the map $\hat{\phi}$:

Lemma 9. *The boundedness of the map $\hat{\phi}$ is equivalent to the boundedness of the radii in any circle pattern.*

Proof. Note that $\hat{\phi}(\mathcal{G}^*)$ is defined up to an additive constant. To get $\hat{\phi}(\mathcal{G}^*)$ from $\phi(\mathcal{G}^*)$ one can chose a root face $\phi(b_0)$ and fold the plane along every edge of the embedding. Note that two adjacent vertices of a circle pattern corresponding to $b, w \in \mathcal{G}$ are symmetric with respect to the edge $\phi((wb)^*)$. Therefore they coincide after one folds the plane along $\phi((wb)^*)$. Hence each circle pattern corresponds to a single point under the mapping $\hat{\phi}$, and the radii in the circle pattern are distances from this point to vertices of $\hat{\phi}(\mathcal{G}^*)$. To finish the proof note that the boundedness of these distances is equivalent to the boundedness of the map $\hat{\phi}$. □

We now explain when $\hat{\phi}$ is bounded.

Lemma 10. *If (λ_1, λ_2) is an interior simple zero, then $\hat{\phi}$ is bounded.*

Proof. Assume first that neither of λ_1, λ_2 is real and fix a dual vertex $u \in \tilde{\mathcal{G}}^*$. We have

$$\hat{\phi}(u + 2p_1) - \hat{\phi}(u + p_1) = \lambda_1 \bar{\lambda}_1^{-1} (\hat{\phi}(u + p_1) - \hat{\phi}(u)).$$

Since $|\lambda_1 \bar{\lambda}_1^{-1}| = 1$, the segment $\hat{\phi}(u + p_1)\hat{\phi}(u + 2p_1)$ differs from $\hat{\phi}(u)\hat{\phi}(u + p_1)$ by a rotation around the center of the circle $C_{u,1}$ through $\hat{\phi}(u)\hat{\phi}(u+p_1)\hat{\phi}(u+2p_1)$ with angle $\arg \lambda_1 \bar{\lambda}_1^{-1} \neq 0$. In particular this implies all the $\hat{\phi}(u + kp_1)$ for $k \in \mathbb{Z}$ lie on $C_{u,1}$. A similar argument holds for $\hat{\phi}(u + kp_2)$. So all the dual vertices $\hat{\phi}(u + k_1 p_1 + k_2 p_2)$ with $(k_1, k_2) \in \mathbb{Z}^2$ have distance at most the sum of the diameters of these two circles from $\hat{\phi}(u)$ and thus lie in a compact set.

Assume now that λ_1 is real and λ_2 is non-real; then $\hat{\phi}$ is periodic in the direction of p_1 and almost periodic in the direction of p_2. We claim that this is possible only if the period in the direction of p_1 is zero: on the one hand the four points $\hat{\phi}(u)$, $\hat{\phi}(u + p_1)$, $\hat{\phi}(u + p_2)$ and $\hat{\phi}(u + p_1 + p_2)$ form a parallelogram (maybe degenerate) because of the periodicity in the direction of p_1, and on the other hand, the vectors $\hat{\phi}(u)\hat{\phi}(u+p_1)$ and $\hat{\phi}(u+p_2)\hat{\phi}(u+p_1+p_2)$ differ by multiplication by $\lambda_2 \bar{\lambda}_2^{-1} \neq 1$, so these vectors must be zero. Therefore $\hat{\phi}$ is also bounded in this case. □

Lemma 11. *For real nodes on the spectral curve, there is a one parameter family of embeddings ϕ, up to similarity, but exactly one of them has a bounded $\hat{\phi}$. Moreover, boundedness of $\hat{\phi}$ is equivalent to the biperiodicity of the radii in any circle pattern.*

Proof. This proof is due to Dmitry Chelkak. Denote by a_1, a_2 the corresponding periods of ϕ and by b_1, b_2 the periods of the map $\hat{\phi}$. Note that for each u, v in the unit disk $u, v \in \mathbb{D}$ the pair of functions $(F + u\bar{F}, G + v\bar{G})$ also defines, via (8), a non-degenerate embedding $\phi_{u,v}$: a black face of $\phi_{u,v}$ is the images of a black face b of ϕ under the linear map $z \mapsto z + v\bar{z}$, followed by a homothety with factor $\frac{F(b)+u\bar{F}(b)}{F(b)}$. Similarly the white faces undergo the linear map $z \mapsto z + u\bar{z}$ followed by a homothety; these linear maps have positive determinant when $u, v \in \mathbb{D}$, and so preserve orientation (and convexity).

If we let $a = na_1 + ma_2$ a period of ϕ and $b = nb_1 + mb_2$ a period of $\hat{\phi}$, then the corresponding period of $\phi_{u,v}$ is $a + u\bar{b} + vb + uv\bar{a}$. Thus we need

$$a + u\bar{b} + vb + uv\bar{a} \neq 0 \text{ for all } u, v \in \mathbb{D}. \tag{13}$$

Note that $a + u\bar{b} + vb + uv\bar{a} = 0$ when $u = -\frac{bv+a}{v\bar{a}+\bar{b}}$. Under what conditions are there no solutions with $u, v \in \mathbb{D}$? The map $v \mapsto -(bv + a)/(\bar{a}v + \bar{b})$ sends the unit circle to itself, and maps the unit disk strictly outside the unit disk if and only if $|a| \geq |b|$. So the above condition (13) is equivalent to the condition $|a| \geq |b|$ for all n, m. This condition can be further reformulated as follows: the image of $\mathbb{D}$ under the mapping $z \mapsto (a_1 + b_1 z)/(a_2 + b_2 z)$ does not intersect the real line: otherwise, one would have $(a_1 - ta_2) + (b_1 - tb_2)z = 0$ for some real t, a contradiction with $|a| \geq |b|$.

Note that $\hat{\phi}$ is biperiodic. To find a bounded $\hat{\phi}$, we need to find $u, \bar{v} \in \mathbb{D}$ such that the periods of $\phi_{u,v}$ are zero:

$$b_1 + u\bar{a}_1 + \bar{v}a_1 + u\bar{v}\bar{b}_1 = 0$$
$$b_2 + u\bar{a}_2 + \bar{v}a_2 + u\bar{v}\bar{b}_2 = 0$$

or equivalently,

$$\frac{b_1 + \bar{v}a_1}{\bar{a}_1 + \bar{v}\bar{b}_1} = -u = \frac{b_2 + \bar{v}a_2}{\bar{a}_2 + \bar{v}\bar{b}_2}.$$

Both fractional-linear mappings send the unit disk to itself, since $|a_{1,2}| \geq |b_{1,2}|$. Therefore it is enough to show that this quadratic equation in $\bar{v}$ has a root in $\mathbb{D}$; the corresponding u will lie in $\mathbb{D}$ too.

Clearly, either one of the roots is inside the unit disk and the other outside, or both are on the unit circle. Finally, note that the latter is impossible as one would have

$$\frac{\bar{a}_1 + \bar{v}\bar{b}_1}{\bar{a}_2 + \bar{v}\bar{b}_2} = \frac{b_1 + \bar{v}a_1}{b_2 + \bar{v}a_2} = \frac{a_1 + vb_1}{a_2 + vb_2} \in \mathbb{R}$$

which is contradiction with the fact that the image of $\mathbb{D}$ under the mapping $z \mapsto (a_1 + b_1 z)/(a_2 + b_2 z)$ does not intersect the real line.

The last statement follows because when $\hat{\phi}$ is bounded it is biperiodic. □

4.3. **T-graphs for periodic bipartite graphs.** The notion of a T-graph was introduced in [23]. A pairwise disjoint collection $L_1, L_2, \ldots, L_n$ of open line segments in $\mathbb{R}^2$ *forms a T-graph in* $\mathbb{R}^2$ if $\cup_{i=1}^n L_i$ is connected and contains all of its limit points except for some set $R = \{r_1, ..., r_m\}$, where each r_i lies on the boundary of the infinite component of $\mathbb{R}^2 \setminus \overline{\cup_{i=1}^n L_i}$. Elements in R are called root vertices. Starting from a T-graph one can define a bipartite graph, whose black vertices are the open line segments L_i and whose white vertices are the (necessarily convex) faces of the T-graph. A white vertex is adjacent to a black vertex if the corresponding face contains a portion of the corresponding segment as its boundary. Using a T-graph one can define in a natural geometric way (real) Kasteleyn weights on this bipartite graph: the weights are a sign $\pm$ times the lengths of the corresponding segments, where the sign depends on which side of the black segment the white face is on; changing the choice of which side corresponds to the + sign is a gauge change. Conversely, as described in [23], for a planar bipartite graph with Kasteleyn weights one can construct a T-graph corresponding to this bipartite graph. For infinite bi-periodic bipartite graphs one can similarly construct infinite T-graphs without boundary. For any (λ_1, λ_2) in the liquid phase, we consider the realization $\phi_1 : \tilde{\mathcal{G}}^* \to \mathbb{C}$ defined from $\omega(w, b) = \mathrm{Re}(G(w))K(w, b)F(b)$.

Lemma 12. *The realization ϕ_1 defined above is a T-graph embedding.*

Proof. The proof starts along the lines of Theorem 4.6 of [23], which deals with the finite case. The ϕ_1-image of each black face is a line segment. For a generic direction u, consider the inner products $\psi(v) := \phi_1(v) \cdot u$ as v runs over vertices of $\tilde{\mathcal{G}}^*$; we claim that this function ψ satisfies a maximum principle: it has no local maxima or minima. This fact follows from the Kasteleyn matrix orientation: If a face v of $\tilde{\mathcal{G}}$ has vertices $w_1, b_1, \ldots, w_k, b_k$ in counterclockwise order, we denote the neighboring faces as $v_1, v_2, \ldots, v_{2k}$. Then the ratios

$$\frac{\phi_1(v) - \phi_1(v_{2i-1})}{\phi_1(v) - \phi_1(v_{2i})} = \frac{\omega(w_i, b_i)}{-\omega(w_{i+1}, b_i)} = -\frac{\mathrm{Re}(G(w_i))K(w_i, b_i)}{\mathrm{Re}(G(w_{i+1}))K(w_{i+1}, b_i)}$$

(with cyclic indices) cannot be all positive, by the Kasteleyn condition. Thus not all black faces of $\tilde{\mathcal{G}}^*$ adjacent to v have ϕ_1-image with an endpoint at v: at least one has v in its interior and thus there is a neighbor of v with larger value of ψ and a neighbor with smaller value of ψ.

It follows from Remark 6 and Proposition 7 that ϕ_1 is a locally finite realization, in the sense that any compact set contains only finitely many points of the form ϕ_1. Indeed, in the real node case, $2\phi_1 = \phi + \hat{\phi}$ is periodic of nonzero period while in the interior simple zero case, it is the sum of the periodic realization ϕ of nonzero period and of the realization $\hat{\phi}$ which is bounded by Lemma 10.

We claim that the ϕ_1 image of a white face w of is a convex polygon. If not, we could find a vector u and four vertices v_1, v_2, v_3, v_4 of w in clockwise order such that both $\psi(v_1), \psi(v_3)$ are larger than either of $\psi(v_2), \psi(v_4)$. By the maximum principle we can then find four disjoint infinite paths starting from v_1, v_2, v_3, v_4 respectively on which $\psi(v)$ is respectively increasing, decreasing, increasing, decreasing. We linearly extend ϕ_1 in order to define it on the edges of $\tilde{\mathcal{G}}^*$. Consider a circle $\mathcal{C}$ such that the disk that

it bounds contains $\phi_1(v_i)$ for all $1 \leq i \leq 4$. By the local finiteness property, this disk contains finitely many points of the realization ϕ_1, hence the four paths must intersect $\mathcal{C}$. Denoting by A_i the point at which the i-th path intersects $\mathcal{C}$ for the first time for $1 \leq i \leq 4$, we obtain that $\psi(A_1), \psi(A_3)$ are larger than either of $\psi(A_2), \psi(A_4)$, which contradicts the convexity of $\mathcal{C}$ and completes the proof of the claim that the ϕ_1-image of each white face is convex.

A similar argument applied to the black segments shows that the set of white faces adjacent to a black segment winds exactly once around the black segment, rather than multiple times, so ϕ_1 is a local embedding near a black segment.

Since ϕ_1 is also locally finite, it has to be proper hence it is a global embedding. □

4.4. **Correspondence.** Let $\mathcal{G}$ be a bipartite graph on the torus, with an equivalence class of positive edge weights under gauge equivalence. The weights are said to define a *liquid phase* if the amoeba of P has the origin in its interior [21]. In this case there is either an interior pair of conjugate simple roots $(\lambda_1, \lambda_2), (\bar{\lambda}_1, \bar{\lambda}_2)$ satisfying $|\lambda_1|, |\lambda_2| = 1$, or a real node $(\lambda_1, \lambda_2) = (\pm 1, \pm 1)$.

By Theorem 8 above, associated to the data of a liquid phase dimer model is a periodic, orientation preserving convex embedding ϕ of $\mathcal{G}^*$, well defined up to homothety and translation. The converse is also true, giving us a bijection between these spaces:

Theorem 13. *For toroidal graphs, the correspondence between liquid phase dimer models and periodic circle center embeddings is bijective.*

Proof. Given a periodic, orientation-preserving embedding ϕ of $\tilde{\mathcal{G}}^*$ satisfying the angle condition (and thus a convex embedding), we define edge weights by associating to each edge e in $\tilde{\mathcal{G}}$ the complex number corresponding to the dual edge e^* dual to e, oriented in such a way that the white dual face lies on its left. These edge weights define positive X variables, because the sum of black angles equals the sum of white angles around each dual vertex.

Let K be the associated Kasteleyn matrix, with $K(w, b)$ equal to the corresponding complex edge weight. Then we we see that K is in a canonical gauge, since the sum of the $K(w, b)$ around each vertex is zero.

It remains to see that the weights are in a liquid phase. Since all face weights are real, K is gauge equivalent to a matrix $K_0(\lambda_1, \lambda_2)$, which has real weights except on the dual curves γ_1, γ_2 where the weights are multiplied by $\lambda_1^{\pm 1}, \lambda_2^{\pm 1}$ as before. Thus $K = GK_0F$ for some functions G, F. If at least one of λ_1, λ_2 is nonreal, then (λ_1, λ_2) is an interior zero of P, so we are in a liquid phase. If λ_1, λ_2 are both real, then K_0 is real; in this case K_0 must have two dimensional kernel: both $\mathrm{Re}(F)$ and $\mathrm{Im}(F)$ are in the kernel, and $\mathrm{Re}(G)$ and $\mathrm{Im}(G)$ are in the left kernel; since the embedding is two-dimensional either $\mathrm{Re}(F)$ and $\mathrm{Im}(F)$ are independent vectors or $\mathrm{Re}(G)$ and $\mathrm{Im}(G)$ are independent vectors. Thus (λ_1, λ_2) is at a real node of P and again we are in a liquid phase. □

5. Spider move, central move and Miquel dynamics

5.1. **A central relation.** Given five distinct points $u, u_1, u_2, u_3, u_4 \in \mathbb{C}$, consider the following equation for an unknown z:

$$\frac{(u_2 - z)(u_4 - z)}{(u_1 - z)(u_3 - z)} = \frac{(u_2 - u)(u_4 - u)}{(u_1 - u)(u_3 - u)}. \tag{14}$$

This quadratic equation has two roots $z = u$ and $z = \tilde{u}$ where

$$\tilde{u} = \frac{uu_1u_3 - u_1u_2u_3 - uu_2u_4 + u_1u_2u_4 - u_1u_3u_4 + u_2u_3u_4}{uu_1 - uu_2 + uu_3 - u_1u_3 - uu_4 + u_2u_4}. \tag{15}$$

We call the map $u \mapsto \tilde{u}$ *a central move*.

The central relation is known to be an integrable discrete equation of octahedron type. Rewriting (15) yields

$$\frac{(u - u_1)(u_2 - \tilde{u})(u_3 - u_4)}{(u_1 - u_2)(\tilde{u} - u_3)(u_4 - u)} = -1$$

which coincides with type χ_2 in the Adler-Bobenko-Suris list [1] and arises in the classical Menelaus theorem in projective geometry [24].

The central move depends on four other points u_1, u_2, u_3, u_4. It is related to the following circle pattern relation: Suppose we have circles C, C_1, C_2, C_3, C_4 centered at u, u_1, u_2, u_3, u_4 with, for $i = 1, 2, 3, 4$, the triple of circles C, C_i, C_{i+1} meeting at a point. Then, by Miquel's six circles theorem [30], there is another circle $\tilde{C}$ which, for each $i = 1, 2, 3, 4$ intersects C_i, C_{i+1} at the other point of intersection of C_i and C_{i+1}. This circle $\tilde{C}$ has center $\tilde{u}$.

Theorem 14 (Centers of Miquel's six circles)**.** *Suppose five circles have centers u, u_1, u_2, u_3, u_4 as in Figure 4. Then the center $\tilde{u}$ of the remaining circle through $\tilde{A}, \tilde{B}, \tilde{C}, \tilde{D}$ coincides with the point given by the central move* (14)*.*

Proof. The existence of the sixth circle follows from Miquel's six circles theorem. It remains to show the relation between the centers. Notice that the line connecting two centers is always perpendicular the common chord of the two circles. The center of the sixth circle is determined uniquely as the intersection of the perpendicular bisectors of $\tilde{A}\tilde{B}, \tilde{B}\tilde{C}, \tilde{C}\tilde{D}, \tilde{D}\tilde{A}$. It suffices to show that the point $\tilde{u}$ determined from (15) lies on these perpendicular lines.

We show that $\tilde{u} - u_2$ is perpendicular to $\tilde{A} - \tilde{B}$. On one hand, since $\tilde{A}, \tilde{B}, B, A$ are concyclic, their cross ratio is real. We know that $u_3 - u_2 \perp \tilde{B} - B$, $u - u_2 \perp B - A$, $u_1 - u_2 \perp A - \tilde{A}$. Thus we have $\tilde{u} - u_2 \perp \tilde{A} - \tilde{B}$ if and only if $\frac{(\tilde{u}-u_2)(u-u_2)}{(u_1-u_2)(u_3-u_2)}$ is real. On the other hand, since u, u_1, u_2, u_3, u_4 are circumcenters, the quantity $X := -\frac{(u_2-u)(u_4-u)}{(u_1-u)(u_3-u)}$ is real. Considering the quadratic equation (14), the roots $u, \tilde{u}$ satisfy

$$u + \tilde{u} = \frac{(u_2 + u_4) + X(u_1 + u_3)}{1 + X}, \quad u\,\tilde{u} = \frac{u_2u_4 + Xu_1u_3}{1 + X} \tag{16}$$

and hence

$$\frac{(\tilde{u} - u_2)(u - u_2)}{(u_1 - u_2)(u_3 - u_2)} = X/(1 + X)$$

is real. This implies $\tilde{u} - u_2$ is perpendicular to $\tilde{A} - \tilde{B}$.

Similarly we can show that $\tilde{u}$ lies on the other perpendicular lines and so $\tilde{u}$ is the circumcenter of the sixth circle. □

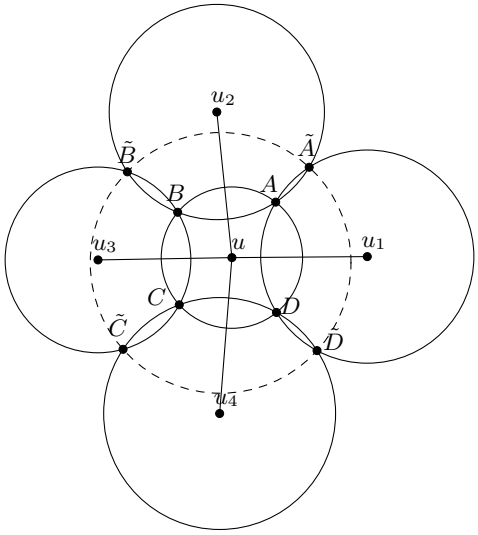

FIGURE 4. Miquel's six circles theorem states that given a configuration of five circles, meeting three at a time at A, B, C, D as indicated, there exists a sixth circle (dotted in the diagram) passing through the four remaining intersection points. The circumcenters of the six circles satisfy the central relation (14).

5.2. **Cluster variables.** Given $u, u_1, u_2, u_3, u_4 \in \mathbb{C}$, we define $X = -\frac{(u_2-u)(u_4-u)}{(u_1-u)(u_3-u)}$. More generally, if we have a bipartite circle pattern with circle centers $\{u_i\}$, and f is a face of degree $2k$, define

$$X_f = -\frac{(u_2-u)(u_4-u)\dots(u_{2k}-u)}{(u_1-u)(u_3-u)\dots(u_{2k-1}-u)}.$$

As discussed in Section 3.2 above, this associates a real variable to every face (i.e. circle) of the circle pattern.

Theorem 15. *Suppose we have a circle pattern with bipartite graph $\mathcal{G}$, and f is a quad face of $\mathcal{G}$, with neighboring faces f_1, f_2, f_3, f_4. Let u, u_1, u_2, u_3, u_4 be the corresponding circle centers, and $X_1, \dots, X_4$ be the X variables. Then under a spider move the circles undergo a Miquel transformation, the new circle center is $\tilde{u}$, and the X variables are transformed as cluster 'Y' variables* [10]*, that is,*

$$\begin{aligned} X' &= X^{-1} \\ X_1' &= X_1(1+X) \\ X_2' &= X_2(1+X^{-1})^{-1} \end{aligned} \tag{17}$$

$$X_3' = X_3(1+X)$$
$$X_4' = X_4(1+X^{-1})^{-1}$$

Proof. Equation (16) implies

$$(\tilde{u}-u_i)(u-u_i) = \frac{u_2u_4 + Xu_1u_3}{1+X} - u_i\frac{(u_2+u_4)+X(u_1+u_3)}{1+X} + u_i^2.$$

This factors for $i = 1, 2, 3, 4$, yielding

$$\frac{(\tilde{u}-u_i)(u-u_i)}{(u_{i+1}-u_i)(u_{i-1}-u_i)} = \begin{cases} 1/(1+X) & \text{for odd i} \\ 1/(1+X^{-1}) & \text{for even i.} \end{cases} \tag{18}$$

Now (17) is a short verification. □

5.3. **Miquel dynamics.** Miquel dynamics is a dynamical system on circle patterns with the combinatorics of the square grid [34]. We color the faces (corresponding to circles) black and white in a chessboard fashion. A black mutation is to remove all the black circles and replace them by new circles obtained from Miquel's theorem, and similarly for a white mutation. More precisely, black (resp. white) mutation moves each vertex to the other intersection point of the two white (resp. black) circles it belongs to. Applying two mutations of the same type gives the identity map. Miquel dynamics is the process of applying black and white mutations alternately on a circle pattern. Our notion of the central move shows that the centers under Miquel dynamics follow an integrable system equivalent to that of the octahedron recurrence (defined in [11]).

Note that, while Miquel dynamics was originally defined as a dynamics on circle patterns, it is also a well-defined dynamics on centers of circle patterns. In terms of centers $u : F(\mathbb{Z}^2) \to \mathbb{C}$, a *black mutation* M_b simply applies a central move to all black centers. In terms of spider moves on (the dual graph) $\mathbb{Z}^2$, a black mutation can be decomposed into two steps:

Step 1: Apply a spider move to the black faces.
Step 2: Contract all the degree-2 vertices.

The new black centers and the old white centers define a map $M_b(u) : F(\mathbb{Z}^2) \to \mathbb{C}$ giving the centers of the circle pattern $M_b(z)$. Similarly one defines the white mutation M_w. Applying black and white mutations alternately yields a sequence of square grids

$$\{\dots, M_b(M_w(u)), M_w(u), u, M_b(u), M_w(M_b(u)), \dots\}$$

As in section 5.2, a weight $X : F(\mathbb{Z}^2) \to \mathbb{R}_{>0}$ is associated to the centers of the circle pattern.

Proposition 16. *Under a black mutation*

$$M_b(X_{m,n}) = \begin{cases} X_{m,n}^{-1} & \text{if } (m,n) \text{ is a black face} \\ X_{m,n}\frac{(1+X_{m,n+1})(1+X_{m,n-1})}{(1+X_{m+1,n}^{-1})(1+X_{m-1,n}^{-1})} & \text{if } (m,n) \text{ is a white face} \end{cases}$$

In particular, $X > 0$ if and only if $M_b(X) > 0$. The same holds for a white mutation.

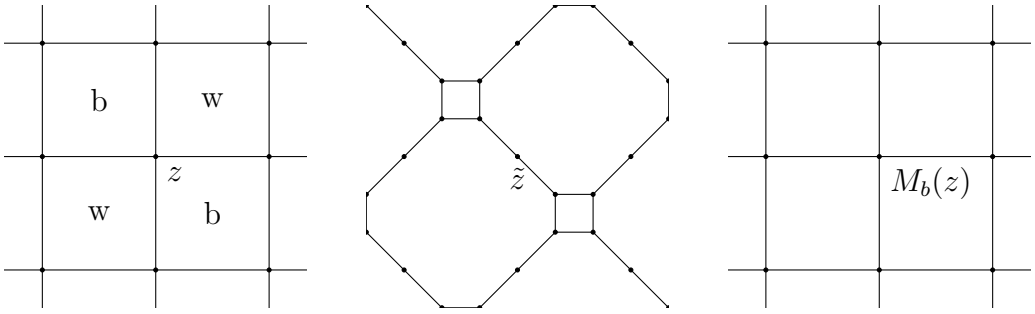

FIGURE 5. Starting with $z : \mathbb{Z}^2 \to \mathbb{C}$ with black and white faces (Left), a black mutation M_b applied a spider move to each black face (Center). We then contract all the degree-2 vertices and obtain a new immersion $M_b(z) : \mathbb{Z}^2 \to \mathbb{C}$ (Right).

Proof. The formulas follow from Theorem 15. If $X > 0$, the equations yield $M_b(X) > 0$ immediately. If $M_b(X) > 0$, then $X = M_b(M_b(X)) > 0$. □

This implies that the class of circle patterns with positive face weights is preserved under Miquel dynamics.

The class of spatially biperiodic circle patterns is also preserved by Miquel dynamics [34] and in that case, Miquel dynamics is integrable and one can deduce a complete set of invariants from the partition function of the underlying dimer model [13].

5.4. **Fixed points of Miquel dynamics.** In this subsection we study the fixed points of Miquel dynamics. Given a circle pattern, one can construct its centers and given the centers, one can compute the X variables. This gives three possible definitions of "fixed point of Miquel dynamics", in increasing order of strength: either the collection of X variables is preserved, or the collection of centers is preserved, or the circle pattern itself is preserved.

We first consider the case of a center being fixed by the central move. We rewrite the central move (Eq. 15) as follows:

Lemma 17. *Suppose* $X := -\frac{(u_1-u)(u_3-u)}{(u_2-u)(u_4-u)} > 0$. *If* $u_1 - u_2 + u_3 - u_4 \neq 0$, *we have*

$$\tilde{u} = u + \frac{((u_1-u)(u_3-u) - (u_2-u)(u_4-u))^2 - (u_1-u_2)(u_2-u_3)(u_3-u_4)(u_4-u_1)}{((u_1-u)(u_3-u) - (u_2-u)(u_4-u))(u_1-u_2+u_3-u_4)}$$

If $u_1 - u_2 + u_3 - u_4 = 0$, *we have*

$$\tilde{u} = u + \frac{(u_1-u) + (u_2-u) + (u_3-u) + (u_4-u)}{2}.$$

Recall that a tangential quadrilateral is a quadrilateral with an incircle, i.e. a circle tangent to the extended lines of the four sides. The incircle is unique if it exists. In this case, the center of the incircle is the intersection of bisectors of interior angles at the four corners.

Proposition 18. *Suppose* $X = -\frac{(u_2-u)(u_4-u)}{(u_1-u)(u_3-u)} > 0$. *Then the quadratic equation* (14) *has a repeated root* $u = \tilde{u}$ *if and only if* $u_1u_2u_3u_4$ *forms a tangential quadrilateral with an incircle centered at* u.

Proof. If $u_1 - u_2 + u_3 - u_4 = 0$, then setting $\tilde{u} = u$ in Lemma 17 implies

$$u = \frac{u_1 + u_3}{2} = \frac{u_2 + u_4}{2}.$$

is the center of the parallelogram $u_1u_2u_3u_4$. Furthermore X being positive implies the parallelogram is a rhombus whose incircle is centered at u.

Otherwise, we assume $u_1 - u_2 + u_3 - u_4 \neq 0$. Lemma 17 implies the segment $u\,u_i$ is an angle bisector of $\angle u_{i-1}u_iu_{i+1}$. To see this, setting $\tilde{u} = u$ in Lemma 17 yields

$$u_4 = -\frac{(u-u_1)(u-u_2)(u-u_3)}{(u-u_2)^2 - (u_3-u_2)(u_1-u_2)} + u$$

Substituting it into X, we have

$$X = -\frac{(u_2-u)(u_4-u)}{(u_1-u)(u_3-u)} = \frac{(u-u_2)^2}{-(u-u_2)^2 + (u_3-u_2)(u_1-u_2)}.$$

Since X is positive, we can deduce $\frac{(u_3-u_2)(u_1-u_2)}{(u-u_2)^2} = \frac{1}{X} + 1$ is positive as well and thus the segment $u\,u_2$ is an angle bisector of $\angle u_1u_2u_3$. Similarly we can deduce that u lies on the angles bisectors of the other three corners and hence there is an incircle tangent to $u_1u_2u_3u_4$ and centered at u. □

We can now characterize the centers that are preserved under the Miquel dynamics.

Theorem 19. *The centers of a circle pattern are preserved under Miquel dynamics if and only if they are also the centers of some circle pattern where diagonal circles are tangential, i.e. the circles centered at* $u_{m,n}$ *and* $u_{m+1,n+1}$ *are tangential, and the circles centered at* $u_{m,n}$ *and* $u_{m-1,n+1}$ *are tangential.*

Proof. Suppose the centers $u : F(\mathbb{Z}^2) \to \mathbb{C}$ are fixed under the central move. Then Proposition 18 implies that $u_{m,n}$ is at the center of the inscribed circle of the quadrilateral $u_{m+1,n}u_{m,n+1}u_{m-1,n}u_{m,n-1}$.

We define $z : \mathbb{Z}^2 \to \mathbb{C}$ to be the intersection of the diagonals in each elementary quadrilateral $u_{m,n}u_{m+1,n+1} \cap u_{m+1,n}u_{m,n+1}$. We claim the faces of z are cyclic, centered at the u's. To see this it suffices to show that $z_r := u_{m,n}u_{m+1,n+1} \cap u_{m,n+1}u_{m+1,n}$ is the image of $z_l := u_{m,n}u_{m-1,n+1} \cap u_{m,n+1}u_{m-1,n}$ under the reflection across $u_{m,n}u_{m,n+1}$. This indeed holds because of Proposition 18 since under the reflection the ray $u_{m,n}u_{m+1,n+1}$ from $u_{m,n}$ through $u_{m+1,n+1}$ is the image of the ray $u_{m,n}u_{m-1,n+1}$ while the ray $u_{m,n+1}u_{m+1,n}$ is the image of the ray $u_{m,n+1}u_{m-1,n}$.

Now consider the circles defined by the faces of the z's; this is a *new* set of circles centered at the u's (not those inscribed in the quadrilaterals). We claim that the diagonal circles are tangent to each other. To see this, consider the point z_0 which is the intersection of the diagonals $u_{m,n}u_{m+1,n+1} \cap u_{m+1,n}u_{m,n+1}$. Notice that the distance between z_0 and $u_{m,n}$ is the radius of the circle at $u_{m,n}$ and similarly the distance between z_0 and $u_{m+1,n+1}$ is the radius of the circle at $u_{m+1,n+1}$. Since z_0 lies on the line

joining $u_{m,n}$ and $u_{m+1,n+1}$, which is perpendicular to both circles, the opposite circles are tangential. □

A particular case where opposite circles are tangential is the case of circle patterns with constant intersection angle. For a circle pattern $z : V(\mathbb{Z}^2) \to \mathbb{C}$, one can measure the intersection angle $\theta : E(\mathbb{Z}^2) \to [0, \pi)$ between neighboring circles. We say a circle pattern has *constant horizontal and vertical intersection angles* if there exists $\alpha \in [0, \pi/2]$ such that

$$\theta = \begin{cases} \alpha & \text{along vertical edges} \\ \pi - \alpha & \text{along horizontal edges} \end{cases}$$

It is an *orthogonal circle pattern* if $\alpha = \pi/2$, see [36].

Corollary 20. *Suppose $u : \mathbb{Z}^2 \to \mathbb{C}$ gives the centers of a circle pattern with constant intersection angle α and z is some other circle pattern with u as centers. Then the orbit of every intersection point z of the circle pattern lies on a circle, and $M_b \circ M_w$ rotates the point around the circle by angle 2α.*

Proof. For each elementary quad $Q = u_{m,n}u_{m+1,n}u_{m+1,n+1}u_{m,n+1}$, the diagonals intersect at angle α. We denote $\tilde{z}_0$ the intersection of the diagonals while z_0 is the intersection of the circles at $u_{m,n}u_{m+1,n}u_{m+1,n+1}u_{m,n+1}$. Generally, $z_0 \neq \tilde{z}_0$ unless z is the circle pattern of constant intersection angle. Applying a Miquel's move M_w once, $\tilde{z}_0$ is fixed while z_0 is reflected across one of the diagonals to $M_w(z_0)$. Applying a black mutation M_b, the point is reflected across the other diagonal. In both cases, the distance to $\tilde{z}$ is preserved. Hence the orbit of z_0 lies on a circle centered at $\tilde{z}_0$.

Thus z_0 is reflected successively across two lines (emanating from $\tilde{z}_0$) meeting at angle α; two such reflections define a rotation around $\tilde{z}_0$ of angle 2α. □

Corollary 21. *A circle pattern is preserved under Miquel dynamics if and only if it has constant horizontal and vertical intersection angles.*

In the infinite planar case, the intersection angles between neighboring circles do not determine the pattern, hence there is a large class of diagonally tangent patterns, which form a one-parameter deformation of the class of orthogonal circle patterns studied by [36]. In the case of spatially biperiodic patterns of prescribed periods, or equivalently, circle patterns on a flat torus, the intersection angles do characterize the circle pattern up to similarity [5], so that the only spatially biperiodic diagonally tangent patterns are those corresponding to regular rectangular grids (all the columns have the same width and all the rows have the same height). Hence in the spatially biperiodic case, the regular rectangular grids are the only fixed points of Miquel dynamics, seen either as a dynamics on circle patterns or on circle centers. The X variables of a given such fixed point are the same for all the faces (equal to the squared aspect ratio of the rectangle formed by a face).

For general, not necessarily biperiodic patterns we have the following.

Proposition 22. *Suppose a circle pattern has face weights $X : F(\mathbb{Z}^2) \to \mathbb{R}_{>0}$. If the centers are preserved under Miquel dynamics, then*

$$X_{m,n}^2 = \frac{(1 + X_{m+1,n}^{-1})(1 + X_{m-1,n}^{-1})}{(1 + X_{m,n+1})(1 + X_{m,n-1})}. \tag{19}$$

Proof. This follows from Proposition 16 and the fact that the labeling of the black and white vertices switches. □

We showed that the centers of a circle pattern with constant intersection angles are fixed by the central moves and hence their X variables satisfy Eq. (19). The converse might not be true; it would be interesting to find all these examples.

Question: Characterize circles patterns with X variables satisfying Eq. (19).

5.5. **Integrals of motion for Miquel dynamics.** Miquel dynamics seen as a dynamics on circle centers on an m by n square grid on the torus corresponds to the dimer urban renewal dynamics on the same graph, which is a finite-dimensional integrable system [13]. The integrals of motion of the dimer dynamics have an interpretation in terms of partition functions for dimer configurations with a prescribed homology and it would be interesting to find a geometric interpretation (in terms of circle patterns) of all these integrals of motion.

It was shown in [34] that the sum along any zigzag loop of intersection angles of circles is an integral of motion. This sum can actually be rewritten as the sum of the turning angles along a dual zigzag loop, which is equal to twice the argument of the alternating product along a primal zigzag loop of the associated complex edge weights. Thus by Theorem 13 the conservation of the sum of angles along zigzag loops implies the invariance under Miquel dynamics of the point on the dimer spectral curve associated with the circle centers.

6. From planar networks to circle patterns

6.1. **Harmonic embeddings of planar networks.** A *circular planar network* is an embedded planar graph $\mathcal{G} = (V, E, F)$, with a distinguished subset $B \subset V$ of vertices on the outer face called boundary vertices, and with a conductance function $c : E \to \mathbb{R}_{>0}$ on edges. Associated to this data is a Laplacian operator $\Delta : \mathbb{C}^V \to \mathbb{C}^V$ defined by

$$\Delta f(v) = \sum_{w \sim v} c_{vw}(f(v) - f(w)).$$

An embedding $f : V \to \mathbb{C}$ is *harmonic* if $\Delta f(v) = 0$ for $v \in V \setminus B$. Harmonic embedding of planar networks arise in various contexts: resistor networks, equilibrium stress configurations, and random walks.

Let $\mathcal{G}$ be a circular planar network, with boundary consisting of vertices $B = \{v_1, \ldots, v_k\}$ on the outer face. The dual $\mathcal{G}^*$ is a graph which is dual to $\mathcal{G}$ in the usual sense except that $\mathcal{G}^*$ has k outer vertices, one between each pair of boundary vertices of $\mathcal{G}$. $\mathcal{G}^*$ is also a circular planar network with boundary B^* consisting of these outer vertices.

Let P be a convex k-gon with vertices $z_1, \dots, z_k$. One can find a function $z : V \to \mathbb{C}$ harmonic on $V \setminus B$ and with values z_i at v_i for $i = 1, \dots, k$. Then z defines a harmonic embedding of $\mathcal{G}$, also known as the Tutte embedding, see [38].

We can also define a harmonic embedding of the dual graph $\mathcal{G}^*$ (harmonic on $\mathcal{G}^* \setminus B^*$) as follows. If z_1 and z_2 are two primal vertices and z_1' (resp. z_2') denotes the dual vertex associated with the face to the right (resp. left) of the edge $z_1 z_2$ when traversed from z_1 to z_2, then we set

$$z_2' - z_1' = i c_{z_1 z_2} (z_2 - z_1).$$

Since the function z is harmonic, this defines a unique embedding of the dual $\mathcal{G}^*$ once one fixes the position of a single dual vertex. This embedding of the dual graph is also harmonic with respect to the inverse conductance (one should take $c_{z_1' z_2'} = c_{z_1 z_2}^{-1}$). Each primal edge is orthogonal to its corresponding dual edge, hence the pair constituted of the harmonic embeddings of the primal and the dual graph form a pair of so-called *reciprocal figures*.

6.2. **From harmonic embeddings to circle patterns.** There is a map from a circular planar network $\mathcal{G}$ to a bipartite graph $\mathcal{G}_H$ with face weights, known as Temperley's bijection [22]: To every vertex and every face of $\mathcal{G}$ is associated a black vertex of $\mathcal{G}_H$. To every edge of $\mathcal{G}$ is associated a white vertex of $\mathcal{G}_H$. A white vertex and a black vertex of $\mathcal{G}_H$ are connected if the corresponding edge in $\mathcal{G}$ is adjacent to the corresponding vertex or face in $\mathcal{G}$. Every bounded face of $\mathcal{G}_H$ is a quadrilateral consisting of two white vertices and two black vertices as in the middle of Fig. 6. Note that the planar network $\mathcal{G}$ has edge weights $c_e = \ell_{e^*}/\ell_e$ where ℓ_e is the distance between the primal vertices and ℓ_{e^*} the distance between the dual vertices. In [22], the induced edge weight on an edge of $\mathcal{G}_H$ which is a half-edge of a dual edge of $\mathcal{G}$ is always set to 1 while an edge of $\mathcal{G}_H$ which is a half-edge of a primal edge e of $\mathcal{G}$ has weight c_e. Thus the bipartite graph has face weights

$$X_f = c_{e_1}/c_{e_2}$$

where e_1, e_2 are two consecutive edges of $\mathcal{G}$ adjacent to face f of $\mathcal{G}_H$. For these weights the partition function of the planar network on $\mathcal{G}$ is equal to the partition function of the dimer model on $\mathcal{G}_H$ up to a multiplicative constant [22].

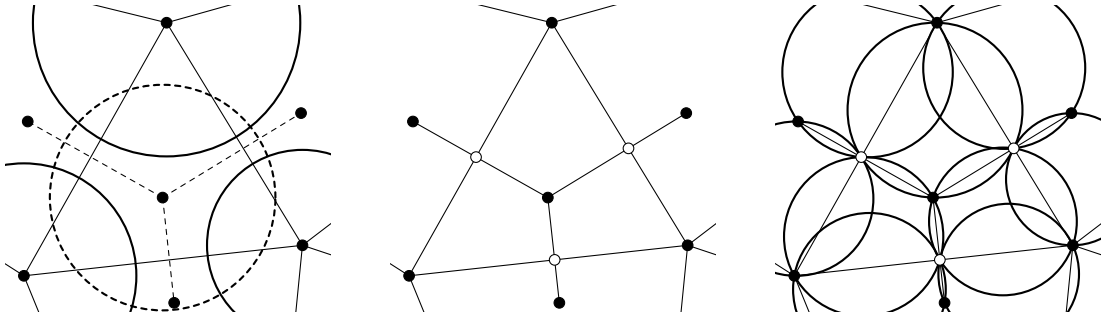

FIGURE 6. From the vertices of reciprocal figures to a circle pattern.

In this section we convert a reciprocal figure into a circle pattern in such a way that the following diagram commutes:

$$\begin{array}{ccc} \text{Planar network } \mathcal{G} & \longrightarrow & \text{Bipartite graph } \mathcal{G}_H \\ \updownarrow & & \updownarrow \\ \text{Reciprocal figure} & \longrightarrow & \text{Circle pattern} \end{array}$$

Theorem 23. *Let $f : V(\mathcal{G}) \to \mathbb{C}$ be a harmonic embedding of a planar network $\mathcal{G}$ in a convex polygon P; let $g : F(\mathcal{G}) \to \mathbb{C}$ be its dual. We define a realization $z : V(\mathcal{G}_H) \to \mathbb{C}$ of the bipartite graph $\mathcal{G}_H$ such that $z = f$ for the black vertices coming from the vertices of $\mathcal{G}$ and $z = g$ for those from the faces of $\mathcal{G}$. On the white vertices, we take z as the intersection of the line through the primal edge and the line through the dual edge under f and g. Then z has cyclic faces and thus is a circle pattern with the combinatorics of $\mathcal{G}_H$. The face weights induced on $\mathcal{G}_H$ from the circle pattern coincide with those from Temperley's bijection.*

Proof. Since every dual edge of $\mathcal{G}$ is perpendicular to its primal edge under the harmonic embeddings, the quadrilateral faces of $\mathcal{G}_H$ have right angles at their white vertices. Hence every face of z is cyclic and hence we obtain a circle pattern. The circumcenter of each cyclic face of z is the midpoint of the two black vertices. By similarity of triangles, the edge weight induced from the distance between circumcenters has the following form: For an edge of $\mathcal{G}_H$ that is a half-edge of a primal edge e of $\mathcal{G}$, it has weight $\ell_{e*}/2$. For an edge of $\mathcal{G}_H$ that is a half-edge of a dual edge e^*, it has weight $\ell_e/2$. Thus for every quadrilateral face ϕ, the face weight is

$$X_\phi = \frac{\ell_{e_1^*}}{\ell_{e_1}} \frac{\ell_{e_2}}{\ell_{e_2^*}} = \frac{c_{e_1}}{c_{e_2}}$$

which coincides with that from Temperley's bijection. □

6.3. **Star-triangle relation.** It is a well-known fact [9] that a network can be reduced to the trivial network by performing star-triangle and triangle-star moves, as well as two other types of moves: replacing two parallel edges (sharing the same endpoints) with a single edge, and replacing two edges in series with a single edge (that is, deleting a degree-2 vertex).

The star-triangle move has a simple interpretation in terms of reciprocal figures: it corresponds exactly to Steiner's theorem (see Figure 6.3), as was observed in [25]. The star-triangle move corresponds to replacing a vertex which is the intersection of three primal edges by a dual vertex which is the intersection of three dual edges; Steiner's theorem guarantees that these three dual edges intersect at a common point.

In [13] it was observed that a $Y - \Delta$ transformation for planar networks can be decomposed into a composition of four urban renewals for dimer models, upon transforming the planar network into a dimer model via Temperley's bijection. We show that this decomposition can be seen in purely geometric terms, using the correspondences between planar networks and reciprocal figures on the one hand, and between dimer models and circle patterns on the other hand.

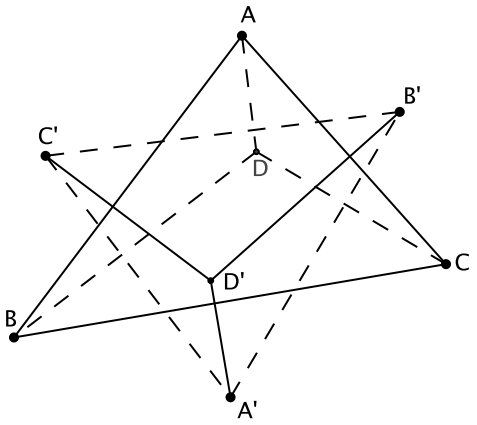

FIGURE 7. Steiner's theorem (see e.g. [3, 4.9.18]) states the perpendicular to (AB) going through C', the perpendicular to (BC) going through A' and the perpendicular to (AC) going through B' are concurrent if and only if the perpendicular to $(A'B')$ going through C, the perpendicular to $(B'C')$ going through A and the perpendicular to $(A'C')$ going through B are concurrent.

Theorem 24. *The star-triangle move for reciprocal figures can be decomposed into four Miquel moves, upon transforming the reciprocal figures into a circle pattern as described in Theorem 23.*

Proof. This decomposition is illustrated in Figure 8. We start with a triangle ABC in a harmonic embedding, we denote by D' the dual vertex associated with that triangle and by A', B' and C' the three dual vertices adjacent to D'. We construct the circle pattern associated with the reciprocal figures as described in Theorem 23, denoting by a', b' and c' the intersections of the primal edges and their associated dual edges. We respectively denote by O_A, O_B and O_C the centers of the circumcircles of the quadrilaterals $Ac'D'b'$, $Ba'D'c'$ and $Cb'D'a'$. We also respectively denote by $O_{AC'}$, $O_{C'B}$, $O_{BA'}$, $O_{A'C}$ $O_{CB'}$ and $O_{B'A}$ the circumcenters of the triangles $Ac'C'$, $C'c'B$, $Ba'A'$, $A'a'C$, $Cb'B'$ and $B'b'A$. We first apply the Miquel move M_{O_C} to the quadrilateral $D'a'Cb'$ with circumcenter O_C. The points D', a', C and b' respectively transform into c', $I_{A'}$, c and $I_{B'}$, which form a cyclic quadrilateral with circumcenter denoted by O. Then we apply the Miquel move M_{O_A} to the quadrilateral $Ac'I_{B'}b'$ with circumcenter O_A. The points A, c', $I_{B'}$ and b' respectively transform into a, I_A, c and B', which form a cyclic quadrilateral with circumcenter denoted by $O_{B'}$. Next we apply the Miquel move M_{O_B} to the quadrilateral $Ba'I_{A'}c'$ with circumcenter O_B. The points B, a', $I_{A'}$ and c' respectively transform into b, A', c and I_B, which form a cyclic quadrilateral with circumcenter denoted by $O_{A'}$. Finally we apply the Miquel move M_O to the quadrilateral $I_Ac'I_Bc$ with circumcenter O. The points I_A, c', I_B and c respectively transform into a, C', b and D, which form a cyclic quadrilateral with circumcenter denoted by $O_{C'}$.

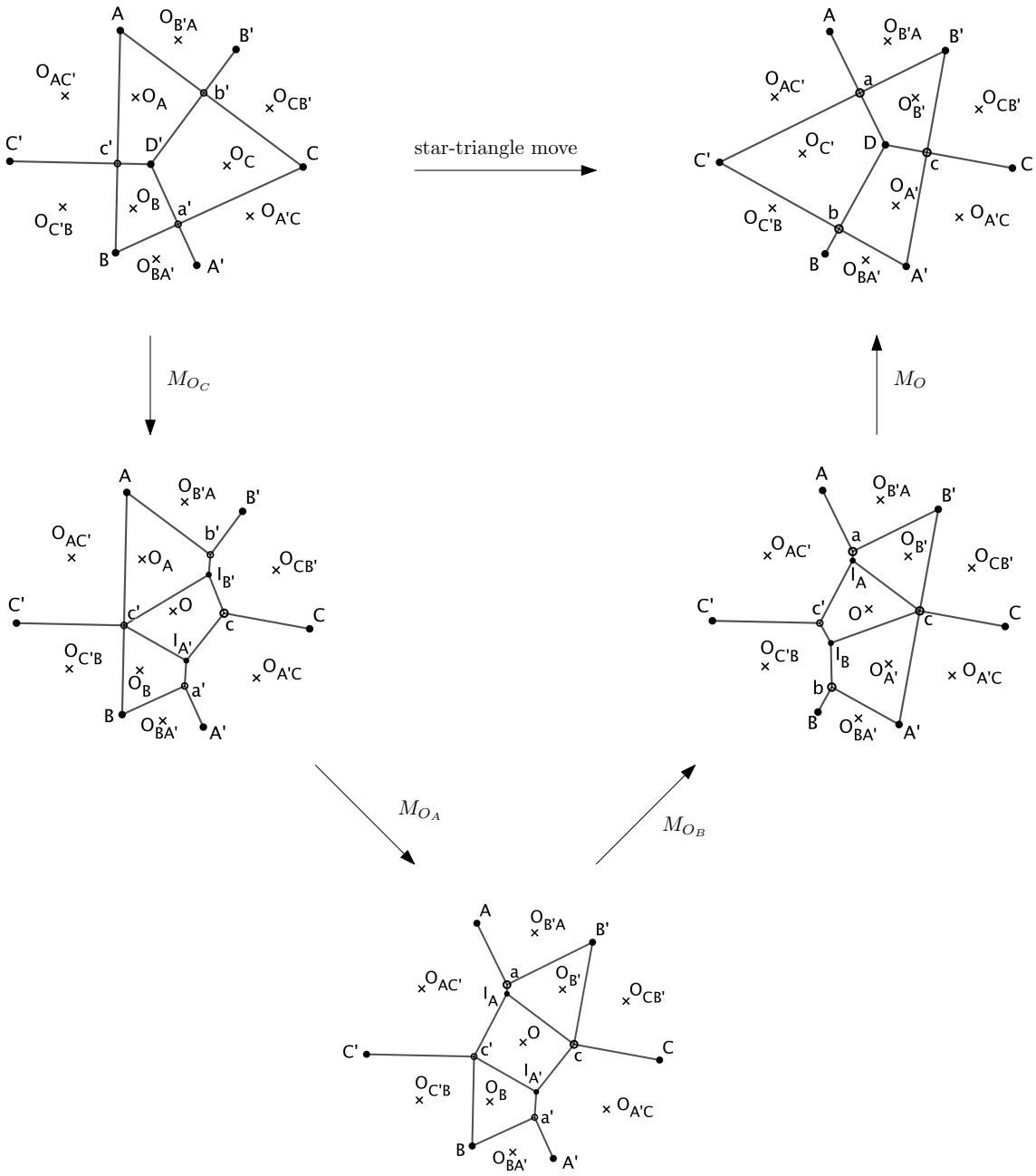

FIGURE 8. Decomposition of a star-triangle move for reciprocal figures into four Miquel moves.

We now show that this point D created by a composition of four Miquel moves coincides with the point $\tilde{D}$ created by the star-triangle move applied to the reciprocal figures. First, as observed in the proof of Theorem 23, in a circle pattern coming from reciprocal figures, the center of each circle is the midpoint of the segment formed by the two black vertices. Since $O_{AC'}$ is the circumcenter of the triangle $AC'a$ and is the

midpoint of $[AC']$, this implies that the perpendicular to $(B'C')$ going through A is the line (Aa). Similarly, (Bb) is the perpendicular to $(A'C')$ going through B and (Cc) is the perpendicular to $(A'B')$ going through C. Hence the point $\tilde{D}$ created by the star-triangle move is the intersection point of the three lines (Aa), (Bb) and (Cc). Because of the orthogonality property at a, b and c, the point $\tilde{D}$ lies on the circumcircles of the three triangles $aC'b$, $bA'c$ and $cB'a$ so $\tilde{D} = D$. □

7. From Ising s-embeddings to circle patterns

We consider the Ising model on a planar graph $\mathcal{G}$ with edge weights x_e, related to the coupling constants $J_e > 0$ by $x_e = \tanh(\beta_c J_e)$, where β_c is the inverse critical temperature. Chelkak introduced in [6] an **s-embedding** of $\mathcal{G}$, which is an embedding s defined on each vertex, dual vertex and edge midpoint of $\mathcal{G}$ with the following property: For any edge e in $\mathcal{G}$, if $v_0^\bullet$ and $v_1^\bullet$ (resp. v_0° and v_1°) denote the endpoints of e (resp. of the edge dual to e) and v_e denotes the midpoint of e as on Figure 9, then $s(v_0^\bullet)$, $s(v_0^\circ)$, $s(v_1^\bullet)$ and $s(v_1^\circ)$ form a tangential quadrilateral with incenter $s(v_e)$, meaning that there exists a circle centered at $s(v_e)$ and tangential to the four sides of the quadrilateral.

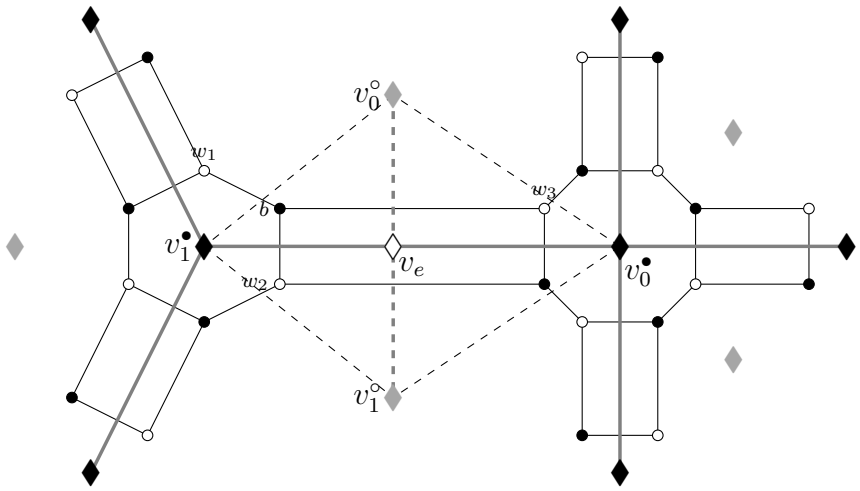

Figure 9. Ising graph $\mathcal{G}$ (black lozenges); dual graph $\mathcal{G}^*$ (gray lozenges); dimer graph $\mathcal{G}_D$ (black and white vertices).

On the other hand, Dubedat [8] gave a natural map from the Ising model on $\mathcal{G}$ to a bipartite dimer model $\mathcal{G}_D$, as in Figure 9: Each edge in $\mathcal{G}$ is replaced by a quadrilateral in $\mathcal{G}_D$ and each vertex or face of degree d in $\mathcal{G}$ is replaced by a face of degree $2d$ in $\mathcal{G}_D$. Every face of $\mathcal{G}_D$ corresponds to a vertex, an edge or a face of $\mathcal{G}$. For every edge e of $\mathcal{G}$, define $\theta_e \in (0, \pi)$ by

$$x_e = \tan \frac{\theta_e}{2}.$$

Then we define the edge weights on $\mathcal{G}_D$ by the following formulas (adopting the notation of Figure 9):

$$\omega(bw_1) = 1, \quad \omega(bw_2) = \cos\theta_e, \quad \omega(bw_3) = \sin\theta_e.$$

For these weights the partition function of the Ising model on $\mathcal{G}$ is equal (up to a multiplicative constant) to the partition function of the dimer model on $\mathcal{G}_D$, see [8].

The goal of this section is to show that the following diagram commutes:

$$\begin{array}{ccc} \text{Ising model on } \mathcal{G} & \longrightarrow & \text{Bipartite graph } \mathcal{G}_D \\ \updownarrow & & \updownarrow \\ \text{s-embedding} & \longrightarrow & \text{Circle pattern} \end{array}$$

In particular, the s-embedding of the vertices, dual vertices and edge midpoints of $\mathcal{G}$ coincides circle centers associated with the bipartite graph $\mathcal{G}_D$. Note that combinatorially this is consistent since each face of $\mathcal{G}_D$ corresponds to either a vertex, a face or an edge of $\mathcal{G}$.

Theorem 25. *An s-embedding of $\mathcal{G}$ provides an embedding of $\mathcal{G}_D^*$ into $\mathbb{C}$ sending each vertex of $\mathcal{G}_D^*$ to the centers of a circle pattern associated with $\mathcal{G}_D$.*

Proof. It suffices to prove that, for each face of the bipartite graph $\mathcal{G}_D$, the alternating product of the edge weights ω induced by s satisfies (3), where X is the face weight of $\mathcal{G}_D$.

First, we check the conditions on the faces of $\mathcal{G}_D$ that correspond to vertices or faces of $\mathcal{G}$. By symmetry, it suffices to consider just a face of $\mathcal{G}$. Let v^* be a vertex of the dual graph of $\mathcal{G}_D$ which corresponds to a face of $\mathcal{G}$ of degree d and denote by $v_{e_1}, v_1, v_{e_2}, v_2, \dots, v_{e_d}, v_d$ the neighbors of v^* in $\mathcal{G}_D^*$ in counterclockwise order, where the vertices of type v_{e_i} correspond to an edge in $\mathcal{G}$ while the vertices of type v_i correspond to a vertex in $\mathcal{G}$. The weight of an edge in $\mathcal{G}_D$ dual to an edge of type $v^*v_{e_i}$ (resp. v^*v_i) is of the form $\sin\theta_i$ (resp. is equal to 1). Hence we need to show the following two formulas:

$$\arg \frac{\prod_{i=1}^d s(v_{e_i}) - s(v^*)}{\prod_{i=1}^d s(v_i) - s(v^*)} = \pi \quad \text{and} \quad \frac{\prod_{i=1}^d |s(v_{e_i}) - s(v^*)|}{\prod_{i=1}^d |s(v_i) - s(v^*)|} = \prod_{i=1}^d \sin\theta_i.$$

By splitting each formula into d equations centered around the edges of type $v^*v_{e_i}$, it suffices to prove the following two formulas, where we are using the notation of Figure 9:

$$\arg \frac{s(v_e) - s(v_0^\circ)}{s(v_0^\bullet) - s(v_0^\circ)} = \arg \frac{s(v_1^\bullet) - s(v_0^\circ)}{s(v_e) - s(v_0^\circ)}, \tag{20}$$

$$\sin^2\theta_e = \frac{|s(v_e) - s(v_0^\circ)|^2}{|s(v_1^\bullet) - s(v_0^\circ)| \cdot |s(v_0^\bullet) - s(v_0^\circ)|}. \tag{21}$$

Formula (20) follows from the fact that $s(v_e)$ is the center of the incircle of the quadrilateral with vertices $s(v_0^\bullet)$, $s(v_0^\circ)$, $s(v_1^\bullet)$ and $s(v_1^\circ)$. For the other formula, we start from formula (6.3) in [6] which implies that

$$\tan^2\theta_e = \frac{|s(v_0^\circ) - s(v_e)| \cdot |s(v_1^\circ) - s(v_e)|}{|s(v_0^\bullet) - s(v_e)| \cdot |s(v_1^\bullet) - s(v_e)|},$$

hence

$$\frac{1}{\sin^2\theta_e} = \frac{|s(v_0^\circ) - s(v_e)| \cdot |s(v_1^\circ) - s(v_e)| + |s(v_0^\bullet) - s(v_e)| \cdot |s(v_1^\bullet) - s(v_e)|}{|s(v_0^\circ) - s(v_e)| \cdot |s(v_1^\circ) - s(v_e)|}. \tag{22}$$

Furthermore, we have the following formula:

$$|s(v_1^\bullet) - s(v_0^\circ)| \cdot |s(v_0^\bullet) - s(v_0^\circ)| = \frac{|s(v_0^\circ) - s(v_e)|}{|s(v_1^\circ) - s(v_e)|} \left(|s(v_0^\circ) - s(v_e)| \cdot |s(v_1^\circ) - s(v_e)| + |s(v_0^\bullet) - s(v_e)| \cdot |s(v_1^\bullet) - s(v_e)|\right), \tag{23}$$

since $s(v_0^\bullet)$, $s(v_0^\circ)$, $s(v_1^\bullet)$ and $s(v_1^\circ)$ form a tangential quadrilateral of incenter $s(v_e)$.

Next, we check these conditions for faces of $\mathcal{G}_D$ corresponding to edges of $\mathcal{G}$. We need to show the following two formulas:

$$\arg \frac{(s(v_0^\bullet) - s(v_e))(s(v_1^\bullet) - s(v_e))}{(s(v_0^\circ) - s(v_e))(s(v_1^\circ) - s(v_e))} = \pi, \tag{24}$$

$$\frac{\cos^2 \theta_e}{\sin^2 \theta_e} = \frac{|s(v_0^\bullet) - s(v_e)| \cdot |s(v_1^\bullet) - s(v_e)|}{|s(v_0^\circ) - s(v_e)| \cdot |s(v_1^\circ) - s(v_e)|}. \tag{25}$$

Formula (24) follows from subdividing the quadrilateral with vertices $s(v_0^\bullet)$, $s(v_0^\circ)$, $s(v_1^\bullet)$ and $s(v_1^\circ)$ into four triangles sharing the common vertex $s(v_e)$, taking the alternating sum of four formulas of the type of (20). Formula (25) follows immediately from formula (6.3) in [6]. □

Acknowledgements

We are grateful to Dmitry Chelkak for sharing his ideas during many fruitful exchanges, and providing the proof of Lemma 11. R. Kenyon is supported by NSF grant DMS-1713033 and the Simons Foundation award 327929. S. Ramassamy acknowledges the support of the Fondation Simone et Cino Del Duca and of the ENS-MHI chair funded by MHI. M. Russkikh is supported by NCCR SwissMAP of the SNSF and ERC AG COMPASP.

References

[1] V. E. Adler, A. I. Bobenko, and Y. B. Suris, *Classification of integrable discrete equations of octahedron type*, Int. Math. Res. Not., (2012), pp. 1822–1889.
[2] N. Affolter, *Miquel dynamics, Clifford lattices and the dimer model*, Preprint, (2018). `http://arxiv.org/abs/1808.04227`.
[3] A. V. Akopyan, *Geometry in figures*, Createspace, 2011.
[4] A. V. Akopyan and A. A. Zaslavsky, *Different views on the isogonal conjugation*, Matematicheskoe prosveshenie, 3 (2007), pp. 61–78.
[5] A. I. Bobenko and B. A. Springborn, *Variational principles for circle patterns and Koebe's theorem*, Trans. Amer. Math. Soc., 356 (2004), pp. 659–689.
[6] D. Chelkak, *Planar Ising model at criticality: state-of-the-art and perspectives*, Preprint, (2017). `http://arxiv.org/abs/1712.04192`.
[7] D. Chelkak, B. Laslier, and M. Russkikh, *Holomorphic functions on t-embeddings of planar graphs*. In preparation.
[8] J. Dubédat, *Exact bosonization of the Ising model*, ArXiv e-prints, (2011).
[9] G. V. Epifanov, *Reduction of a plane graph to an edge by star-triangle transformations*, Dokl. Akad. Nauk SSSR, 166 (1966), pp. 19–22.
[10] V. Fock and A. Goncharov, *Moduli spaces of local systems and higher Teichmüller theory*, Publ. Math. Inst. Hautes Études Sci., (2006), pp. 1–211.

[11] S. Fomin and A. Zelevinsky, *The Laurent phenomenon*, Adv. in Appl. Math., 28 (2002), pp. 119–144.
[12] A. Glutsyuk and S. Ramassamy, *A first integrability result for Miquel dynamics*, J. Geom. Phys., 130 (2018), pp. 121–129.
[13] A. B. Goncharov and R. Kenyon, *Dimers and cluster integrable systems*, Ann. Sci. Éc. Norm. Supér. (4), 46 (2013), pp. 747–813.
[14] A. Grothendieck, *Éléments de géométrie algébrique. IV. Étude locale des schémas et des morphismes de schémas. I*, Inst. Hautes Études Sci. Publ. Math., (1964), p. 259.
[15] T. C. Hull, *The combinatorics of flat folds: a survey*, in Origami^3 (Asilomar, CA, 2001), A K Peters, Natick, MA, 2002, pp. 29–38.
[16] P. W. Kasteleyn, *Graph theory and crystal physics*, in Graph Theory and Theoretical Physics, Academic Press, London, 1967, pp. 43–110.
[17] R. Kenyon, *Local statistics of lattice dimers*, Ann. Inst. H. Poincaré Probab. Statist., 33 (1997), pp. 591–618.
[18] R. Kenyon, *The Laplacian and Dirac operators on critical planar graphs*, Invent. Math., 150 (2002), pp. 409–439.
[19] R. Kenyon, *Lectures on dimers*, in Statistical mechanics, vol. 16 of IAS/Park City Math. Ser., Amer. Math. Soc., Providence, RI, 2009, pp. 191–230.
[20] R. Kenyon and A. Okounkov, *Planar dimers and Harnack curves*, Duke Math. J., 131 (2006), pp. 499–524.
[21] R. Kenyon, A. Okounkov, and S. Sheffield, *Dimers and amoebae.*, Ann. Math. (2), 163 (2006), pp. 1019–1056.
[22] R. W. Kenyon, J. G. Propp, and D. B. Wilson, *Trees and matchings*, Electron. J. Combin., 7 (2000), pp. Research Paper 25, 34.
[23] R. W. Kenyon and S. Sheffield, *Dimers, tilings and trees*, J. Combin. Theory Ser. B, 92 (2004), pp. 295–317.
[24] B. G. Konopelchenko and W. K. Schief, *Menelaus' theorem, Clifford configurations and inversive geometry of the Schwarzian KP hierarchy*, J. Phys. A, 35 (2002), pp. 6125–6144.
[25] ——, *Reciprocal figures, graphical statics, and inversive geometry of the Schwarzian BKP hierarchy*, Stud. Appl. Math., 109 (2002), pp. 89–124.
[26] W. Y. Lam, *Discrete minimal surfaces: critical points of the area functional from integrable systems*, Int. Math. Res. Not. IMRN, (2018), pp. 1808–1845.
[27] M. Lis, *Circle patterns and critical Ising models*, Preprint, (2017). `http://arxiv.org/abs/1712.08736`.
[28] C. Mercat, *Discrete Riemann surfaces and the Ising model*, Comm. Math. Phys., 218 (2001), pp. 177–216.
[29] G. Mikhalkin, *Real algebraic curves, the moment map and amoebas*, Ann. of Math. (2), 151 (2000), pp. 309–326.
[30] A. Miquel, *Théorèmes sur les intersections des cercles et des sphères.*, J. Math. Pures Appl., (1838), pp. 517–522.
[31] C. Müller, *Planar discrete isothermic nets of conical type*, Beiträge zur Algebra und Geometrie / Contributions to Algebra and Geometry, (2015), pp. 1–24.
[32] J. K. Percus, *One more technique for the dimer problem*, J. Mathematical Phys., 10 (1969), pp. 1881–1888.
[33] H. Pottmann and J. Wallner, *The focal geometry of circular and conical meshes*, Adv. Comput. Math., 29 (2008), pp. 249–268.
[34] S. Ramassamy, *Miquel dynamics for circle patterns*, Int. Math. Res. Not., (2018). To appear.
[35] I. Rivin, *Euclidean structures on simplicial surfaces and hyperbolic volume*, Ann. of Math. (2), 139 (1994), pp. 553–580.
[36] O. Schramm, *Circle patterns with the combinatorics of the square grid*, Duke Math. J., 86 (1997), pp. 347–389.

[37] D. P. Thurston, *From dominoes to hexagons*, in Proceedings of the 2014 Maui and 2015 Qinhuangdao conferences in honour of Vaughan F. R. Jones' 60th birthday, vol. 46 of Proc. Centre Math. Appl. Austral. Nat. Univ., Austral. Nat. Univ., Canberra, 2017, pp. 399–414.
[38] W. T. Tutte, *How to draw a graph*, Proc. London Math. Soc. (3), 13 (1963), pp. 743–767.
[39] W. Whiteley, *Rigidity and scene analysis*, in Handbook of discrete and computational geometry, CRC Press Ser. Discrete Math. Appl., CRC, Boca Raton, FL, 1997, pp. 893–916.

Richard Kenyon, Mathematics Department, Brown University, Providence, RI 02912
E-mail address: richard_kenyon at brown.edu

Wai Yeung Lam, Mathematics Department, Brown University, Providence, RI 02912
E-mail address: lam at math.brown.edu

Sanjay Ramassamy, Département de mathématiques et applications, École normale supérieure, 45 rue d'Ulm, 75 005 Paris, France
E-mail address: sanjay.ramassamy at ens.fr

Marianna Russkikh, Section de mathématiques, Université de Genève, 2-4 rue du Lièvre, case postale 64, 1211 Genève 4, Switzerland
E-mail address: marianna.russkikh at unige.ch